Available online at www.sciencedirect.com

ScienceDirect

Palaeoworld 34 (2025) 100902

Palaeoworld

www.elsevier.com/locate/palwor

Upper Cretaceous (Cenomanian–lower Campanian) nannofossils and sequence stratigraphy of southwestern Crimea

Ekaterina Shcherbinina *, Yuri Gavrilov

Geological Institute of the Russian Academy of Sciences, Pyzhevsky 7, Moscow 019017, Russia

Received 29 March 2024; received in revised form 16 October 2024; accepted 20 November 2024
Available online 4 December 2024

Abstract

The first high-resolution study of the Cenomanian to lower Campanian calcareous nannofossils of two most continuous but poor in macrofossils sections of southwestern Crimea allowed the detailed division of these successions on the basis of standard nannofossil zonations and the correlation with Tethyan and Boreal Upper Cretaceous. After initial Cenomanian sea-level fall, nannofossil assemblages increase their abundance and taxonomic diversity toward the end of Cenomanian. The most of the Cenomanian bioevents are recognised in the sedimentary record. The Cenomanian/Turonian transition is the most stratigraphically intricate interval in the Late Cretaceous Crimean basin. The lowest occurrences (LOs) of *Cylindralithus biarcus*, *Quadrum intermedium*, *Eprolithus octopetalus*, *Ahmuellerella octoradiata* are identified in the upper Cenomanian. The highest occurrences (HOs) of some stratigraphically important for this time span taxa like *Corollithion kennedyi*, *Cretarhabdus striatus* and *Axopodorhabdus albianus* are found significantly above the levels defined as relevant subzonal boundaries (UC3e, UC4b and UC5b, respectively). The TOC-rich sediments corresponding to Bonarelli Level (OAE2) is intercalated in the upper part of the upper Cenomanian limestones (undivided interval of UC5c-UC6a subzone/zone). *Helenea chiastia* is scarce in the studied succession and its HO cannot be used for definition of zonal boundary (UC6) and the base of Turonian. The most reliable bioevent closest to the Cenomanian/Turonian boundary in this basin is the LO of *Eprolithus moratus* (base of UC6b subzone). The middle Turonian to lower Campanian nannofossil assemblages display the succession of the main bioevents similar to those in Tethyan basin, but show earlier LOs of *Micula* and *Reinhardtites* in the middle Turonian.

Nannofossil biostratigraphy revealed the stratigraphic range of hiatuses in this sedimentary record. Being combined with the levels of the major facies changes, these levels enabled the recognition of five Cenomanian and four Turonian sequence boundaries consistent with the sequence stratigraphy established for Europe. Two sharp erosional surfaces occurred in the upper part of the studied succession correspond to the Coniacian KCo1 and Santonian KSa2 sequences.

Keywords: Biostratigraphy; stratigraphic hiatus; sequence boundary; Cretaceous; northeastern Peri-Tethys

1. Introduction

Upper Cretaceous sediments are widespread in southern Crimea, where they form the middle part of the Second Range of Crimean Mountains showing southwest to northeast strike (Fig. 1A, B). They represent carbonate succession accumulated in the wide shelf of northeastern Peri-Tethys (Fig. 1C). In the southeastern Crimea, the Upper Cretaceous sediments comprise rhythmically built Cenomanian marls and limestones formed in the deeper environment under control of orbital (precessional) (Naydin, 2004) or dissolution (Gabdullin, 2002; Baraboshkin and Zibrov, 2012) cycles and more homogenous shallowing upward

* Corresponding author.
E-mail address: katuniash@gmail.com (E. Shcherbinina).

https://doi.org/10.1016/j.palwor.2024.11.010

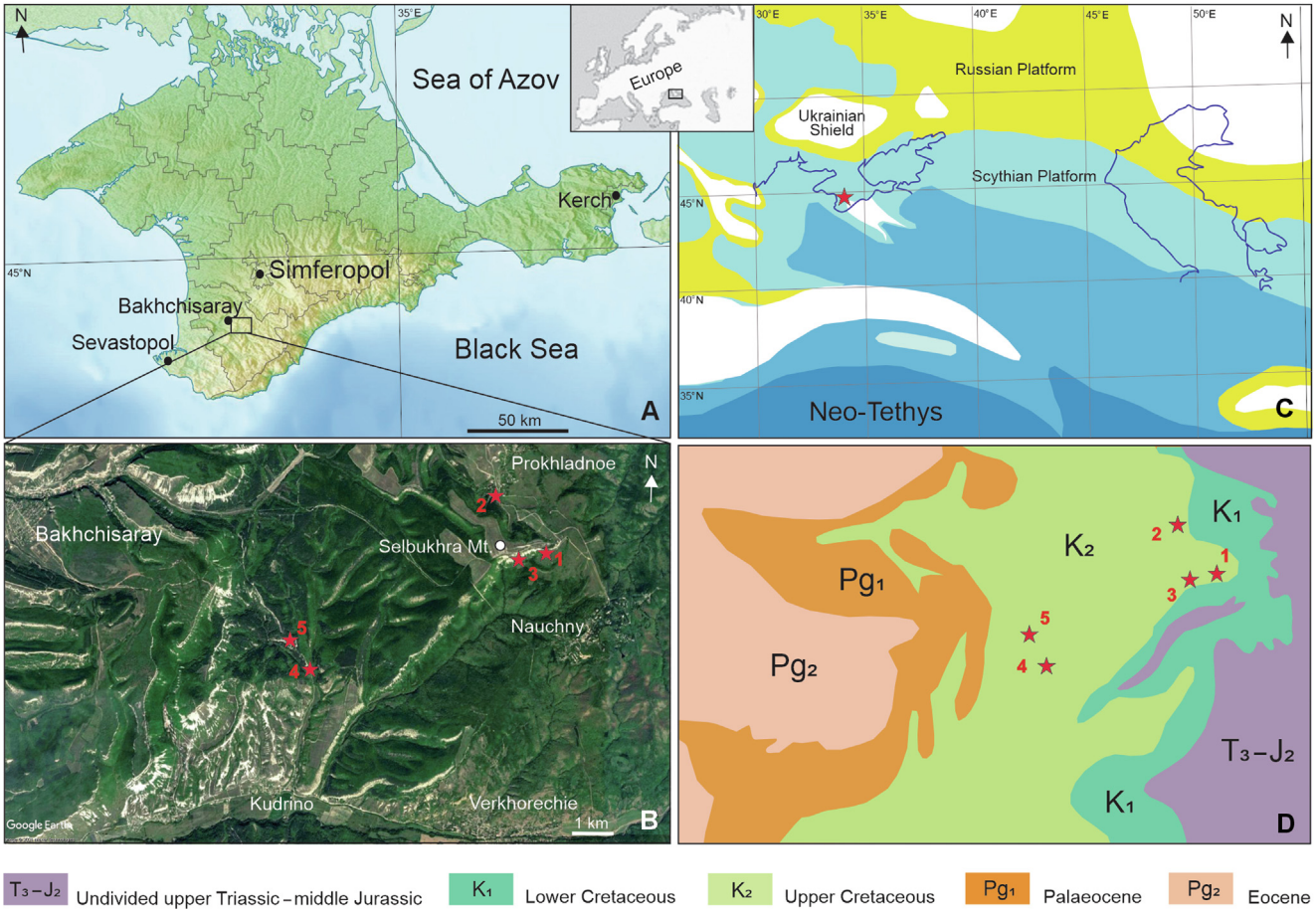

Fig. 1. Location of the studied outcrops in the modern geography (A, B), palaeogeographic (C, modified from Kazmin and Natapov, 1998) and geological (D, modified from Yudin, 2018) maps. (B, D) 1–3 – outcrops of the uppermost Albian to lower Turonian sediments in the southern and northern slopes of Selbukhra Mountain; 4, 5 – outcrops of the upper Cenomanian to lower Campanian sediments in Aksudere ravine.

Turonian-Coniacian succession. The mid-Santonian deepening of the basin resulted in the accumulation of highly calcareous middle Santonian to Campanian sediments. The relatively shallow depth of accumulation and active local tectonics caused the formation of a series of hiatuses of different stratigraphic range and significant basin-wide variation in thickness of the Upper Cretaceous lithologic bodies.

In southwestern Crimea, the Cenomanian marly sediments onlap the upper Albian carbonate sandstones with erosional contact. The most complete Upper Cretaceous succession forms the upper part of the modern Kacha High located in the upper reaches of Belbek, Kacha, and Alma Rivers south- and southeastward of the town of Bakhchisaray. The outcrops of the Upper Cretaceous sediments of Kacha High represent key sections for the western part of Crimea-Caucasus basin. These sediments are poor in ammonites, crinoids, and belemnites; inoceramids irregularly occur in peculiar intervals. The scarcity of the most important macrofossils for the Upper Cretaceous stratigraphy, especially in the Cenomanian to Turonian successions, prompted extensive study of abundant and diverse planktonic foraminifera and calcareous nannofossils. The earlier microfossil studies elucidated the primary importance of planktonic foraminifera for the Upper Cretaceous stratigraphy (Maslakova, 1959, 1978; Dolitskaya, 1972; Kopaevich and Kuzmicheva, 2002; Benyamovsky and Kopaevich, 2016; Kopaevich and Vishnevskaya, 2016; etc.). However, only few studies considering the Upper Cretaceous nannofossil stratigraphy have been carried out in the Crimea (Shumenko and Stetsenko, 1978; Kalinichenko, 1983; Matveev, 2013; Shcherbinina and Gavrilov, 2016; Vishnevskaya et al., 2018; Ustinova and Gabdullin, 2019; Guzhikov et al., 2021; Ovechkina et al., 2021). During the last decades, the multiple studies of microfossils (mainly foraminifera and radiolaria) from the specific levels of the Upper Cretaceous of Kacha High were performed (Kopaevich and Walaszczyk, 1993; Bragina, 1999; Gale et al., 1999; Kuzmicheva, 2001; Alekseev et al., 2007; Guzhikov et al., 2021). However, no systematic study of the Upper Cretaceous stratigraphy using standard nannofossil zonations was made in this key area until now.

This work presents the results of the calcareous nannofossil study of the two most complete sections of Kacha High composing continuous Cenomanian to lower Campa-

nian succession, which allowed the recognition of the standard nannofossil zones (Sissingh, 1977 with additions of Perch-Nielsen, 1985; Burnett, 1998). The observations of the variations in nannofossil assemblages through time and detailed stratigraphy enable the interregional correlation of the Upper Cretaceous sediments and events and provide the basis for further palaeoenvironmental interpretations.

2. Geological and lithostratigraphic setting

The Upper Cretaceous sediments conformably overlie the upper Albian rocks in the territory of southwestern Crimea, forming a monocline of 10–15° northwest dipping. The Albian/Cenomanian transition is featured by short hiatus resulted from the erosion of uppermost Albian sediments. The Cenomanian–lower Campanian succession is mostly composed of marls and limestones integrated into four formations: Belogorsk Formation (Cenomanian), Mender Formation (Turonian), Prokhladnoe Formation (Coniacian), and Kudrino Formation (Santonian–Campanian). The intercalations of dark thinly laminated calcareous clays and marls occur in the lower–middle Cenomanian (up to 2% TOC), uppermost Cenomanian (> 7% TOC), and lower to middle Turonian (1% TOC) (Fig. 2). The measurements of TOC content were made in the Chemical Analysis Laboratory of Geological Institute of the Russian Academy of Sciences from the samples collected by authors from the sections considered in this paper.

A detailed lithological description of the Upper Cretaceous sediments of Kacha High was given by Alekseev (1989), who defined 24 lithostratigraphic units correlatable over southwestern Crimea. The Cenomanian Belogorsk Formation (ca. 64 m) consists of rhythmic alternation of laminated marls and massive compact limestones overlying the upper Albian calcareous sandstones (Fig. 2A). The lower Cenomanian is built up by the alternation of grey calcareous shales and massive light grey silty marls, divided into units I to IV-1 according to the silt content and proportion between the thickness of laminated and massive layers (Alekseev, 1989; Fig. 2B). This succession is extensively bioturbated and contains small pyrite concretions and rare inoceramids. The Subunit IV-2 onlaps the erosional surface at the top of the Subunit VI-1 and contains calcareous pebble at the basal layer. The middle Cenomanian Unit V includes a series of intercalations of TOC-rich dark grey thinly laminated marls containing common pyrite concretions; few centimeter thick bentonite layers occur in the uppermost part of this Unit (Fig. 2C). The upper Cenomanian (Unit VI) is divided into three subunits. The Subunit VI-1 is composed of pale limestones and marls and Subunit VI-2 is built up of compact silty and siliceous limestones with cherty concretions. The erosional contact of the subunits VI-2 and VI-3 is overlapped by a thin layer of yellowish-green non-calcareous clay covered by TOC-rich dark grey thinly laminated marl without borrowing, which corresponds to Bonarelli Level, or OAE2 (Fig. 2D, E).

The lower part of Turonian Mender Formation consists of pale to grey compact laminated marlstones and siliceous limestones with radiolarians (Bragina, 1999), which onlap uneven surface of the Unit VI. Upsection, indistinctly alternating pale and grey shaly and more compact marls (Fig. 2F, G) built up the units VII to IX. According to Alekseev (1989), these units are distinguished only by occurrence of dispersed siliceous concretions, which are very rare at the studied section, thus they remain undivided in our study. The uppermost Turonian–Coniacian Prokhladnoe Formation (units X–XI) is built up by white in the lower part and greenish and pink compact limestones with stylolites in the upper part (Fig. 2H); this formation contains common well preserved large urchins and inoceramids and displays sharp erosional surface at the top. The studied Santonian–lower Campanian part of the overlapping Kudrino Formation consists of two units: Unit XV is composed of white limestones with few centimeter thick intercalations of greenish calcareous clay and Unit XVI is composed of greenish-grey thinly layered marls.

3. Materials and methods

The study of the Cenomanian to lower middle Turonian nannofossils was made from 166 samples collected in three outcrops in the southern and northern slopes of Selbukhra Mountain. The 13 m thick lower part of outcrop 1 (Fig. 1C) provided 17 samples and the 23 m thick upper part of this outcrop was sampled with higher resolution (82 samples). 24 samples were collected in 13.5 m thick outcrop 2 in the northern slope of the mountain. A compilation of continuous succession from isolated outcrops was made using bentonite layers and the number of limestone/marl couplets. The 15.5 m thick outcrop 3 is located ca. 200 m westward from the outcrop 1. We picked up here 43 samples with higher-resolution sampling at the Cenomanian/Turonian transition.

The upper Cenomanian to lower Campanian sediments were sampled in two locations. The 22 m thick Cenomanian to upper Turonian sediments are exposed in the southeastern slope of Aksudere ravine (outcrop 4, 77 samples). Coniacian to lower Campanian sediments were sampled at outcrop 5 located in the head of the ravine and continued along the country road from the village of Kudrino to the town of Bakhchisaray (18 samples). During the field work, our attention was mainly focused on the intervals of the sediments rich in TOC and they were sampled with higher resolution.

Nannofossils were studied from the smear-slides made from the raw sediments of all samples collected using standard techniques described by Bown and Young (1998). The observation of nannofossils was made under Olympus BX-41 microscope at the magnification 1200× and images were made with Infinity X camera. At least 70 fields of view (FOV) were studied in each smear-slide. The semi-

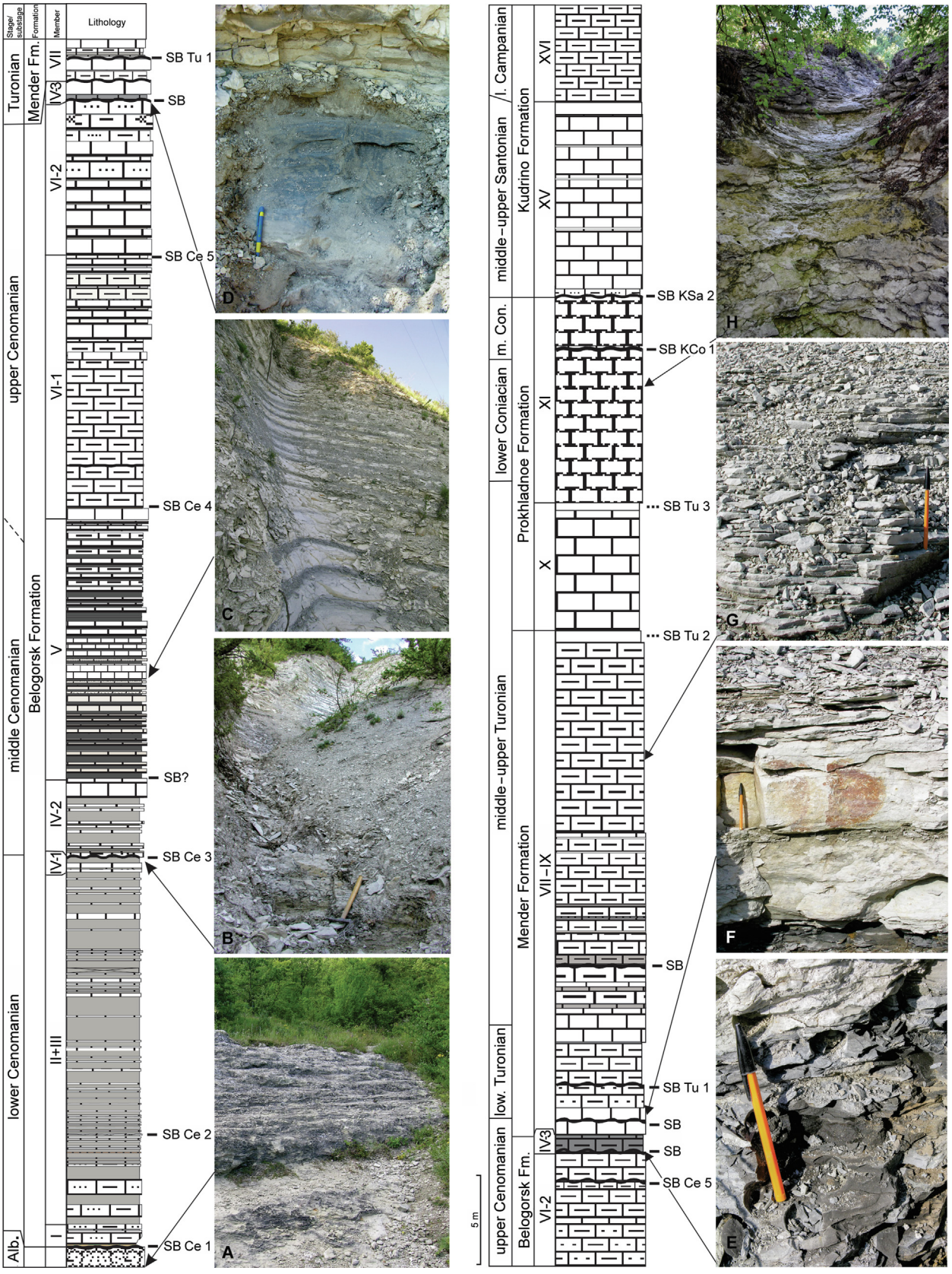

Fig. 2. Lithostratigraphy and field images of the Cenomanian to lower Campanian sediments of Selbukhra (left) and Aksudere (right) sections. (A–C) Outcrop 1. (D) Outcrop 3. (E–G) Outcrop 4. (H) Outcrop 5. Photograph (H) courtesy of A. Guzhikov. Hammer length of (B) is 70 cm, pen length of (D, E–G) is 15 cm. Abbreviations: low. Turonian – lower Turonian, m. Con. – middle Coniacian, l. Campanian – lower Campanian.

quantitative analysis of the species abundance in nannofossil assemblages follows the gradations: abundant – > 5 specimens per FOV of the microscope, common – 1–4 specimens per FOV, few – one to 5–7 specimens in the row of smear-slide, rare – 1–5 specimens per smear-slide.

4. Results

4.1. Nannofossil stratigraphy

Calcareous nannofossils are present in most samples studied, but their total abundance, taxonomic diversity and preservation vary widely. The upper Albian sediments contain very scarce nannofossils and the non-calcareous clay underlying the uppermost Cenomanian black shale (Bonarelli Level) is lack in nannofossils. The mostly medium nannofossil preservation (i.e., the most specimens are identifiable to the genus/species levels with minor dissolution and overgrowth marks) in softer marls becomes worse in the layers of compact limestones due to calcite overgrowing. The most abundant and diverse nannofossil assemblages are identified in the lower to middle Cenomanian, the species richness decreases progressively upward in the section and poor assemblage is observed in the Coniacian compact limestones that is evidently caused by diagenetic recrystallization. Nannofossil total abundance and taxonomical diversity significantly drops in the TOC-rich sediment associated with the terminal Cenomanian OAE2. This can be caused by both primary low nannoplankton abundance and selective dissolution of the most delicate coccoliths. At the same time, there are no pronounced variations in the composition of nannofossil assemblages between middle Cenomanian limestone and TOC-rich marls. The occurrence of a series of stratigraphically important markers enabled the division of the studied sections according to standard zonations of Sissingh (1977) complemented by Perch-Nielsen (1985) and Burnett (1998).

4.1.1. Selbukhra section

The upper Albian sediments of Mangush Formation exposed at the base of outcrop 1 in the southern slope of Selbukhra Mountain (Fig. 3) are almost lack in nannofossils (samples 001 and 002): apart the very rare specimens of *Watznaueria*, which is the most resistant to diagenesis taxon, unique specimens of *Prediscosphaera cretacea* and *Rhagodiscus achlyostaurion* are found. More diverse and abundant nannofossils are observed in the glauconite-rich silty calcareous clay at the base of Cenomanian (sample 003, see Table S1). The co-occurrence of *Corollithion kennedyi*, *Gartnerago nanum* and *G. theta* immediately above this basal layer (sample 004) indicates the interval of UC1a-c subzones. The low diversity assemblage of the lowermost Cenomanian does not allow the recognition of the subzonal boundaries: both marker species for this interval *Watznaueria britannica* and *Gartnerago chiasta* are absent from the section. Possibly, only UC1c subzone, which is above the highest occurrence (HO) of the last species, is present in the section. Thus, the uppermost UC0 to lower UC1 zones are omitted during the initial Cenomanian erosion. The lowest occurrence (LO) of *Helicolithus anceps* (sample 011) denotes the base of UC1d subzone at 5.5 m above the base of Belogorsk Formation. *Gartnerago segmentatum* has late LO in Selbukhra section (in the middle Cenomanian) and the base of UC2 zone cannot be identified. The absence of *Zeugrhabdotus xenotus* from the section does not allow the definition of UC2b subzone. Thus, the interval of UC1d-UC2b remains undivided. At 4.5 m above the LO of *H. anceps*, ca. 13 m thick interval of the section is significantly destroyed by roots and partially covered. This part of section was sampled in the northern slope of Selbukhra Mountain (outcrop 2 in Fig. 1B), where the LO of *Cylindralythus sculptus* (base of UC2c subzone) was found. The rest of Belogorsk Formation was sampled again in the outcrop 1 (southern slope).

The LO of *Lithraphidites acutus* marks the bases of UC3 and CC10 zones; this datum roughly corresponds to the base of the middle Cenomanian. At Selbukhra section, this species has its LO at the level 2.5 m above the erosional surface (Fig. 3). The basal layers of Subunit IV-2 lack of (sample 045) or are very poor (samples 046 and 047) in nannofossils (Table S2), that could result in the slightly later LO of *L. acutus*. The stratigraphic range of the hiatus between lower and middle Cenomanian does not exceed the uppermost part of UC2 zone and lowermost part of UC3 zone. The base of UC3b subzone is defined by the highest occurrence of *Gartnerago theta*. This species is consistently present in the lower Cenomanian of Selbukhra section, but its abundance decreases significantly at ca. 1.5 m above the base of UC3. This level is assumed as a base of UC3b subzone. Above it, rare specimens of *G. theta* persist to be sporadically present up to the uppermost middle Cenomanian.

In the middle Cenomanian, the relative abundance of *Watznaueria* spp. (*W. barnesiae*, *W. biporta*, *W. manivitae*, *W. ovata*) increases, but no significant variations in nannofossil total abundance and species diversity between light and dark members in couplets are observed. Unit V covers the most part of UC3 zone (Fig. 4). Rare specimens of *Quadrum* cf. *intermedium* (Fig. 4DD) appear in the lower part of Unit V and proper *Q. intermedium* with 8 elements (Fig. 4EE) has its LO in the middle of this Unit. The HO of very rare *Staurolithites gausorhethium* approximately defines the top UC3b subzone (Table S3). *Gartnerago nanum*, which was continuously present in the lower Cenomanian, becomes very rare in the Unit V. In this connection, the base of UC3d subzone defined by the LO of this species cannot be recorded with confidence. The rest of the UC3 zone (UC3d-e subzones), embracing the upper part of Unit V and almost the whole Subunit VI-1 (Fig. 5) remains undivided, because *Corollithion kennedyi*, the HO of which denotes the base of UC3e subzone, persists to be continuously present up to the topmost Cenoma-

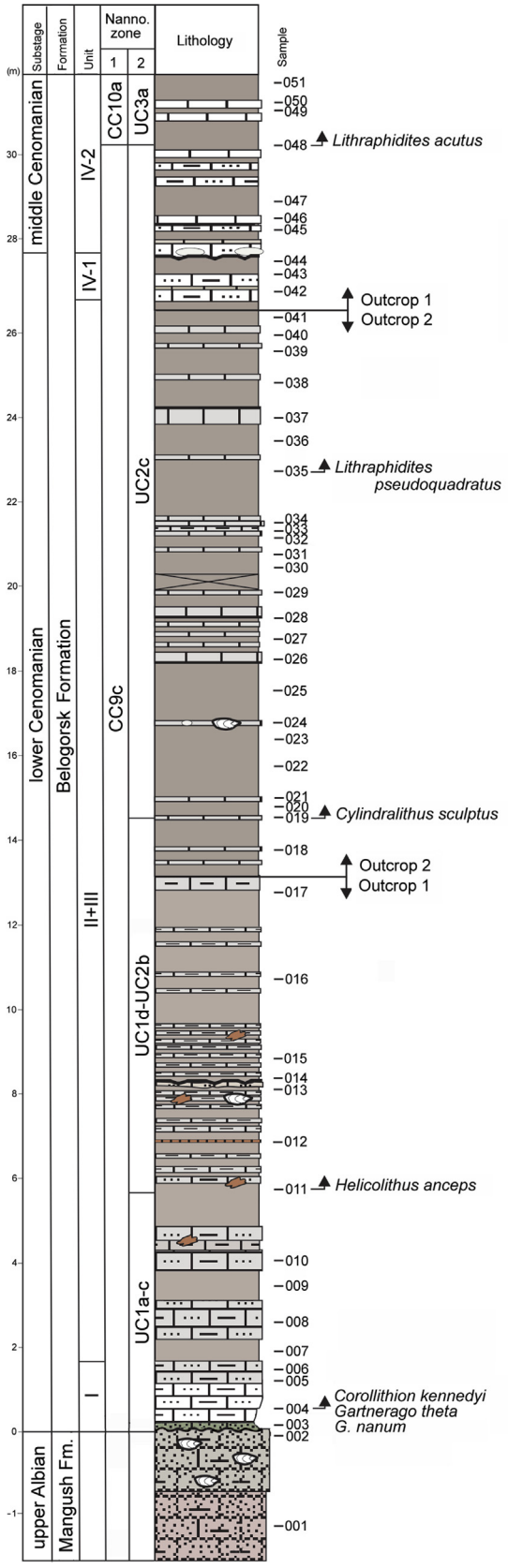
Substage
Formation
Unit
Nanno. zone
1
2
Lithology
Sample
(m)
middle Cenomanian
lower Cenomanian
upper Albian
Belogorsk Formation
Mangush Fm.
IV-2
IV-1
II+III
I
CC10a
UC3a
CC9c
UC2c
UC1d-UC2b
UC1a-c
Lithraphidites acutus
Outcrop 1
Outcrop 2
Lithraphidites pseudoquadratus
Cylindralithus sculptus
Outcrop 2
Outcrop 1
Helicolithus anceps
Corollithion kennedyi
Gartnerago theta
G. nanum

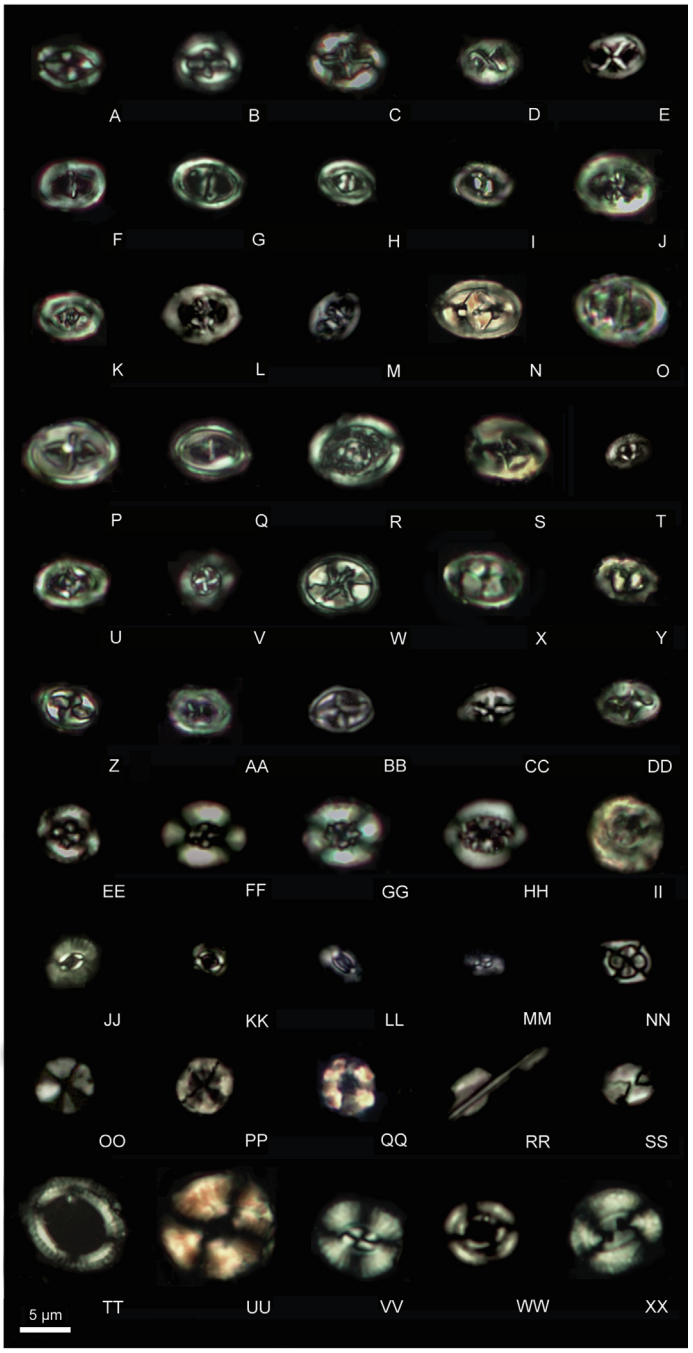
A B C D E
F G H I J
K L M N O
P Q R S T
U V W X Y
Z AA BB CC DD
EE FF GG HH II
JJ KK LL MM NN
OO PP QQ RR SS
TT UU VV WW XX
5 μm

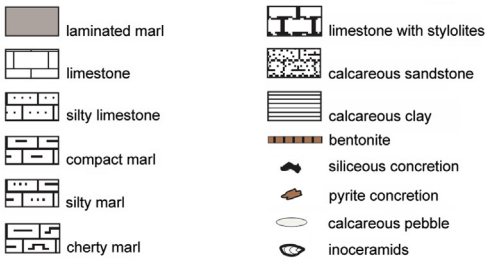
laminated marl
limestone
silty limestone
compact marl
silty marl
cherty marl
limestone with stylolites
calcareous sandstone
calcareous clay
bentonite
siliceous concretion
pyrite concretion
calcareous pebble
inoceramids

nian at Selbukhra section (Table S4). The LO of *Cylindralithus biarcus* at the topmost Subunit VI-1 defines the base of UC4 zone. The early rare specimens of *Quadrum intermedium* with 7 wall-elements are found at this level. The subzones UC4a and UC4b cannot be recognized in Selbukhra section because the last record of *Cretarhabdus striatus* in this section occurs much higher than the HO of *Lithraphidites acutus* (the top of UC4) — at the topmost Cenomanian. The nannofossil assemblage from the interval of the uppermost part of UC3d-e subzone and UC4 zone (samples 129–133) displays lower species richness (15–20 species against 25–35 in underlying sediments) and higher abundance of cool-water *Eprolithus* (*E. floralis* and *E. apertior*).

The base of UC5 zone is denoted by the HO of *Lithraphidites acutus*, which occurs in the middle of Subunit VI-2. The upper part of this zone is featured by successive HOs of *Retecapsa ficula*, *Helicolithus turonicus*, *Eprolithus octopetalus* and LO of *Ahmuellerella octoradiata*. The base of UC5b subzone defined by the HO *Axopodorhabdus albianus* cannot be recognized in Selbukhra section, because this species persists to present up to the lower Turonian (its LO is found above the LO of *Quadrum gartneri*). The base of UC5c subzone corresponds to the LO of *Q. intermedium* with 5 wall-cycle elements in the upper part of Subunit VI-2. The scarcity of *Helenea chiastia* in the Cenomanian succession does not allow precise recognition of its HO, which defines the base of UC6 zone and roughly correlates to the base of Turonian. The small-thickness Subunit VI-3, constrained between two erosional surfaces, ranges the uppermost part of undivided interval of UC5c-6a subzone and UC6b subzone. The black shale layer corresponding to the Bonarelli Level, or OAE2, contains low-diverse nannofossil assemblage of small specimens widely dominated by *Watznaueria*.

The LO of *Eprolithus moratus* ca. 35 cm above the black shale layer denotes the base of UC6b subzone and the LO of *Q. gartneri*, which serves as a base of UC7 and CC11 zones, is found just below the erosional surface at the top of Subunit VI-3. Low diversity of the lower Turonian nannofossil assemblage is likely caused by diagenetic alteration of the compact marlstones and limestones rich in biogenic silica. The LO of *Eiffellithus eximius* marks the base of the middle Turonian UC8 and CC12 zones (Table S5).

4.1.2. Aksudere section

At the base of Aksudere section (outcrop 4 in Fig. 1B), the upper part of the upper Cenomanian Subunit VI-2 is exposed (Fig. 6). Generally, the upper Cenomanian nannofossil assemblage is very similar to that observed at Selbukhra section in this interval (Table S6). The presence of *Cylindralithus biarcus* and *Quadrum intermedium* with 6 and 7 wall-cycle elements and the absence of *Lithraphidites acutus* from the base of the outcrop indicate UC5b and CC10a subzones. *Axopodorhabdus albianus* disappears at Aksudere section at the top of Subunit VI-2, while at Selbukhra section, it has its HO in the Unit VII (above the LO of *Quadrum gartneri*). The LO of *Corollithion kennedyi* is found at the topmost Subunit VI-2 in both sections. *Q. intermedium* with 5 elements appears in sample 46/13 indicating the base of UC5c subzone.

The TOC-rich layer (lower part of Subunit VI-3), ca. 6.0 m above the base of outcrop, is of thicker than that at Selbukhra section (0.6 m versus 0.3 m). The low-abundance and poor taxonomically nannofossil assemblage of this layer is widely dominated by mainly small-sized *Watznaueria barnesiae*. At the same time, heavily calcified *Zeugrhabdotus embergeri* increases its abundance. *Eprolithus* spp. become slightly more abundant in the upper part of the black shale layer. Nannofossils assemblage of the white limestone overlying this bed (upper part of Subunit VI-3) is even of lower diversity, likely, due to calcite overgrowing. *Helenea chiastia* occurs sporadically at Aksudere section and becomes extinct in the upper part

Fig. 3. Litho- and nannofossil stratigraphy of the lower Cenomanian of Selbukhra section and light microscope images of selected nannofossil species under cross polarization. Upward arrows designate LOs of the taxa, downward arrows designate HOs. Nanno. zone – nannofossil zone of Sissingh (1977) with additions of Perch-Nielsen (1985) (1) and Burnett (1998) (2) zonations. (A) *Broinsonia enormis* (Shumenko) Manivit, sample 012. (B) *B. matalosa* (Stover) Burnett, sample 005. (C) *B. signata* Noël, sample 014. (D) *Chiastozygus platyrhethus* Hill, sample 015. (E) *C. litterarius* (Górka) Manivit, sample 010. (F) *Zeugrhabdotus erectus* (Deflandre in Deflandre and Fert) Reinhardt, sample 005. (G) *Z. diplogrammus* (Deflandre in Deflandre and Fert) Burnett, sample 005. (H) *Z. bicrescenticus* (Stover) Burnett, sample 005. (I) *Z. petrizzoae* Bown, sample 005. (J) *Z. scutula* (Bergen) Rutledge and Bown, sample 017. (K) *Z. burwellensis* (Black) Burnett, sample 008. (L) *Z. howei* Bown, sample 015. (M) *Z. xenotus* (Stover) Burnett, sample 033. (N) *Z. embergeri* (Noël) Perch-Nielsen, sample 011. (O) *Gartnerago theta* (Black) Jakubowski, sample 005. (P) *G. nanum* Thierstein, sample 018. (Q) *G. ponticula* Bown and Hampton, sample 010. (R) *Rhagodiscus asper* (Stradner) Reinhardt, sample 005. (S) *R. robustus* Bown, sample 024. (T) *R. achlyostaurion* (Hill) Doeven, sample 005. (U) *R. sageri* Bown, sample 051. (V) *Prediscosphaera columnata* (Stover) Perch-Nielsen, sample 005. (W) *Eiffellithus turriseiffelii* (Deflandre in Deflandre and Fert) Reinhardt, sample 005. (X) *Tranolithus orionatus* Reinhardt, sample 009. (Y) *T. minimus* (Bukry) Perch-Nielsen, sample 017. (Z) *Helicolithus compactus* (Bukry) Varol and Girgis, sample 010. (AA) *H. anceps* (Górka) Noël, sample 011. (BB) *Staurolithites laffittei* Caratini, sample 017. (CC) *S. aenigma* Burnett, sample 009. (DD) *S. gausorhethium* (Hill) Varol and Girgis, sample 042. (EE) *Flabellites oblongus* (Bukry) Crux, sample 050. (FF) *Helenea chiastia* Worsley, sample 005. (GG) *Retecapsa octofenestrata* (Bralower) Bown, sample 005. (HH) *Cretarhabdus conicus* Bramlette and Martini, sample 009. (II) *Cylindralithus sculptus* Bukry, sample 019. (JJ) *Biscutum constans* (Górka) Black, sample 005. (KK) *B. dehiscum* Brace and Watkins, sample 035. (LL) *B. subditivum* Brace and Watkins, sample 009. (MM) *B. aura* Brace and Watkins, sample 009. (NN) *Corollithion kennedyi* Crux, sample 009. (OO) *Radiolithus planus* Stover, sample 035. (PP) *Eprolithus apertior* Black, sample 031. (QQ) *E. floralis* (Stradner) Stover, sample 005. (RR) *Lithraphidites pseudoquadratus* Crux, sample 035. (SS) *Calculites anfractus* (Jakubowski) Varol and Jakubowski, sample 035. (TT) *Manivitella pemmatoidea* (Deflandre) Thierstein, sample 005. (UU) *Watznaueria manivitae* Bukry, sample 048. (VV) *W. barnesiae* (Black) Perch-Nielsen, sample 005. (WW) *W. ovata* Bukry, sample 005. (XX) *W. biporta* Bukry, sample 005.

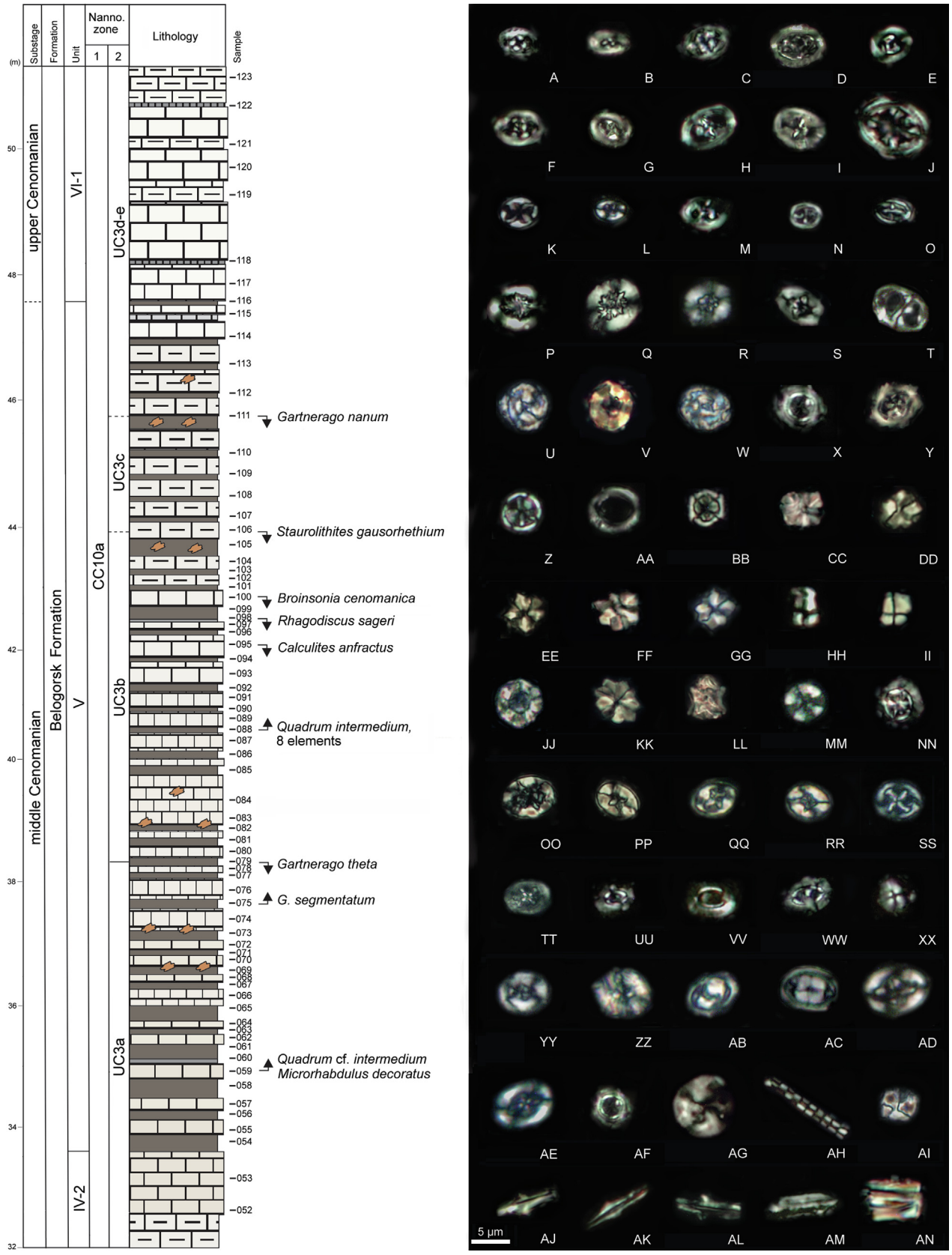
Substage
Formation
Unit
Nanno. zone
1
2
Lithology
Sample
(m)
upper Cenomanian
middle Cenomanian
Belogorsk Formation
VI-1
V
IV-2
CC10a
UC3d-e
UC3c
UC3b
UC3a
Gartnerago nanum
Staurolithites gausorhethium
Broinsonia cenomanica
Rhagodiscus sageri
Calculites anfractus
Quadrum intermedium, 8 elements
Gartnerago theta
G. segmentatum
Quadrum cf. intermedium
Microrhabdulus decoratus
5 µm

of Subunit VI-2 (sample 46/6). Thus, the base of UC6, defined by the HO of this species, cannot be reliably assigned, but the LO of *Eprolithus moratus* at 0.5 m above the black shale indicates the base of the lower Turonian UC6b subzone.

Nannofossil assemblage of the undivided units VII–IX (samples 45/5-2–48/16) is also characterized by low diversity (Tables S6–S8), which drops even more in the dark clayey layers occurred in the lower part of this interval. The thickness of the lower Turonian sequence, albeit containing two hiatuses, is twice as larger than that at Selbukhra section (ca. 5 m against 2.5 m). The LO of *Quadrum gartneri* (the base of UC7) is found 0.7 m above the uppermost Cenomanian black shale. Up the section, the successive LOs of *Helicolithus turonicus*, *Rhagodiscus pancostii* and *Lucianorhabdus maleformis* are observed. *R. pancostii* sporadically occurs up to the middle Turonian. *H. turonicus*, which has its LO at the topmost Cenomanian of Selbukhra section, persists to present up to the top of Turonian.

The LO of *Eiffellithus eximius*, defined the base of UC7, CC11 and the base of the middle Turonian is located 0.7 m above the erosional surface in the lower part of Mender Formation. The middle Turonian nannofossil assemblage is characterized by successive disappearance of *Rhagodiscus* (*R. achlyostaurion*, *R. splendens*, *R. pancostii*, *R. plebeius*), *Cylindralithus* (*C. biarcus*, *C. sculptus*, *C. serratus*) and some *Eprolithus* (*E. apertior* and *E. octopetalus*), which were constantly present in the upper Cenomanian to lower Turonian. At the same time, *Eiffellithus*, *Zeugrhabdotus* and *Quadrum* become more diverse. *Micula* sp. (Fig. 6AN, AO) and *M. adumbrata* (Fig. 7GG) show unexpectedly early occurrence in the lower part of the middle Turonian although the LO of *Micula* genus is commonly referred from the late Turonian. They persist to sporadically present up to the top of Turonian, where they are, albeit rare, consistent representatives of nannofossil assemblage. The lowest presence of very rare *Lucianorhabdus quadrifidus* (the base of UC8b subzone) is detected at the level ca. 8 m above the LO of *E. eximius*. The first specimens of *Reinhardtites* sp. (Fig. 6NN, OO) are found close to this level. The LO of *Lithastrinus septenarius* marking the base of UC9 zone is detected in the upper part of the units VII–IX (sample 48/13). The base of the upper Turonian cannot be recognized at Aksudere section by means of nannofossil study. The HO of *Eprolithus apertior*, the closest to this boundary nannofossil event (Burnett, 1998), is found here much earlier (sample 48/8, UC8b subzone, Table S7) and *Zeugrhabdotus biperforatus*, the LO of which denotes the base of UC9b subzone, is absent from this succession.

At the base of outcrop 5 (Fig. 1B), the upper Turonian/lower Coniacian transition is exposed (Fig. 8). A marker species of UC9c subzone *Broinsonia parca expansa* and *Helicolithus turonicus* are present in the lowermost sample from this exposure (sample 51/1, Table S8), but the last species is absent from the sample taken 1.8 m above it (sample 51/2). According to Lees (2008) and Walaszczyk et al. (2010), the base of Coniacian, defined by the first occurrence of *Cremnoceramus deformis erectus* bivalve, lies just below the HO of *H. turonicus*. Thus, the Turonian/Coniacian boundary falls in the lowermost part of the outcrop 5 in Crimea. *Watznaueria barnesiae*, widely dominated nannofossil assemblage in Cenomanian through middle Turonian, gradually decreases its abundance, while *Lucianorhabdus* and *Micula* underwent several steps of radiation in the Coniacian and younger sediments (Table S9). The LO of *M. staurophora* denotes the bases

Fig. 4. Litho- and nannofossil stratigraphy of the middle to lower upper Cenomanian of Selbukhra section and light microscope images of selected nannofossil species under cross polarization. (A) *Rhagodiscus achlyostaurion* (Hill) Doeven, sample 060. (B) *R. angustus* (Stradner) Reinhardt, sample 080. (C) *R. dekaenelii* Bergen, sample 061. (D) *R. asper* (Stradner) Reinhardt, sample 078. (E) *Gorkaea operio* Varol and Girgis, sample 052. (F) *Zeugrhabdotus howei* Bown, sample 062. (G) *Z. trivectis* Bergen, sample 075. (H) *Z. scutula* (Bergen) Rutledge and Bown, sample 116. (I) *Zeugrhabdotus* sp., sample 076. (J) *Axopodorhabdus albianus* (Black) Wind and Wise, sample 101. (K) *Helicolithus trabeculatus* (Górka) Verbeek, sample 060. (L) *H. leckie* Bown, sample 053. (M) *H. anceps* (Górka) Noël, sample 057. (N) *Staurolithites gausorhethium* (Hill) Varol and Girgis, sample 080. (O) *S. laffittei* Caratini, sample 061. (P) *Cretarhabdus conicus* Bramlette and Martini, sample 076. (Q) *Retecapsa angustiforata* Black, sample 118. (R) *R. ficula* (Stover) Burnett, sample 065. (S) *Bukrylithus ambiguus* Black, sample 064. (T) *Gartnerago theta* (Black) Jakubowski, sample 110. (U) *Cylindralithus serratus* Bramlette and Martini, sample 070. (V) *C. sculptus* Bukry, sample 114. (W) *C. nudus* Bukry, sample 118. (X) *Rotelapillus crenulatus* (Stover) Perch-Nielsen, sample 066. (Y) *Rotelapillus* sp., elliptical *Rotelapillus* with 6 robust radial bars, sample 080. (Z) *Stoverius achylosus* (Stover) Perch-Nielsen, sample 106. (AA) *Loxolithus armilla* (Black) Noël, sample 070. (BB) *Corollithion kennedyi* Crux, sample 118. (CC) *Assipetra terebrodentarius* (Applegate et al.) Rutledge and Bergen, sample 075. (DD) *Quadrum* cf. *intermedium* Varol, sample 088. (EE) *Q. intermedium* Varol, 8 elements, sample 095. (FF, GG) *Q. eneabrachium* Varol; (FF) sample 057; (GG) sample 108. (HH, II) *Quadrum* cf. *bengalensis* Burnett; (HH) sample 115; (II) sample 123. (JJ) *Eprolithus apertior* Black, sample 096. (KK) *E. floralis* (Stradner) Stover, sample 094. (LL) *Eprolithus* sp., side view, sample 117. (MM) *Radiolithus planus* Stover, sample 070. (NN) *Prediscosphaera ponticula* (Bukry) Perch-Nielsen, sample 069. (OO) *Eiffellithus turriseiffelii* (Deflandre in Deflandre and Fert) Reinhardt, sample 091. (PP) *E. gorkae* Reinhardt, sample 092. (QQ) *E. perch-nielseniae* Shamrock in Shamrock and Watkins, sample 123. (RR) *Eiffellithus* cf. *lindiensis* Lees, sample 092. (SS) *Tegumentum stradneri* Thierstein, sample 075. (TT) *Chiastozygus bifarius* Bukry, sample 123. (UU) *Biscutum gaultensis* (Mutterlose) Bown, sample 103. (VV) *Biscutum* cf. *magnum* Wind and Wise, sample 101. (WW) *Biscutum* cf. *thurowii* Burnett, sample 067. (XX) *Discorhabdus ignotus* (Górka) Perch-Nielsen, sample 81. (YY) *Flabellites oblongus* (Bukry) Crux, sample 086. (ZZ) *Helenea chiastia* Worsley, sample 089. (AB) *Tranolithus minimus* (Bukry) Perch-Nielsen, sample 093. (AC) *T. orionatus* Reinhardt, sample 086. (AD) *Broinsonia enormis* (Shumenko) Manivit, sample 086. (AE) *B. cenomanica* (Black) Bown, sample 084. (AF) *Rotelapillus crenulatus* (Stover) Perch-Nielsen, sample 068. (AG) *Haqius circumradiatus* (Stover) Roth, sample 123. (AH) *Microrhabdulus decoratus* Deflandre, sample 123. (AI) *Calculites anfractus* (Jakubowski) Varol and Jakubowski, sample 70. (AJ–AL) *Lithraphidites acutus* Verbeek and Manivit; (AJ) sample 060; (AK) sample 109; (AL) sample 123. (AM) *L. pseudoquadratus* Crux, sample 053. (AN) *Calcicalathina alta* Perch-Nielsen, sample 102.

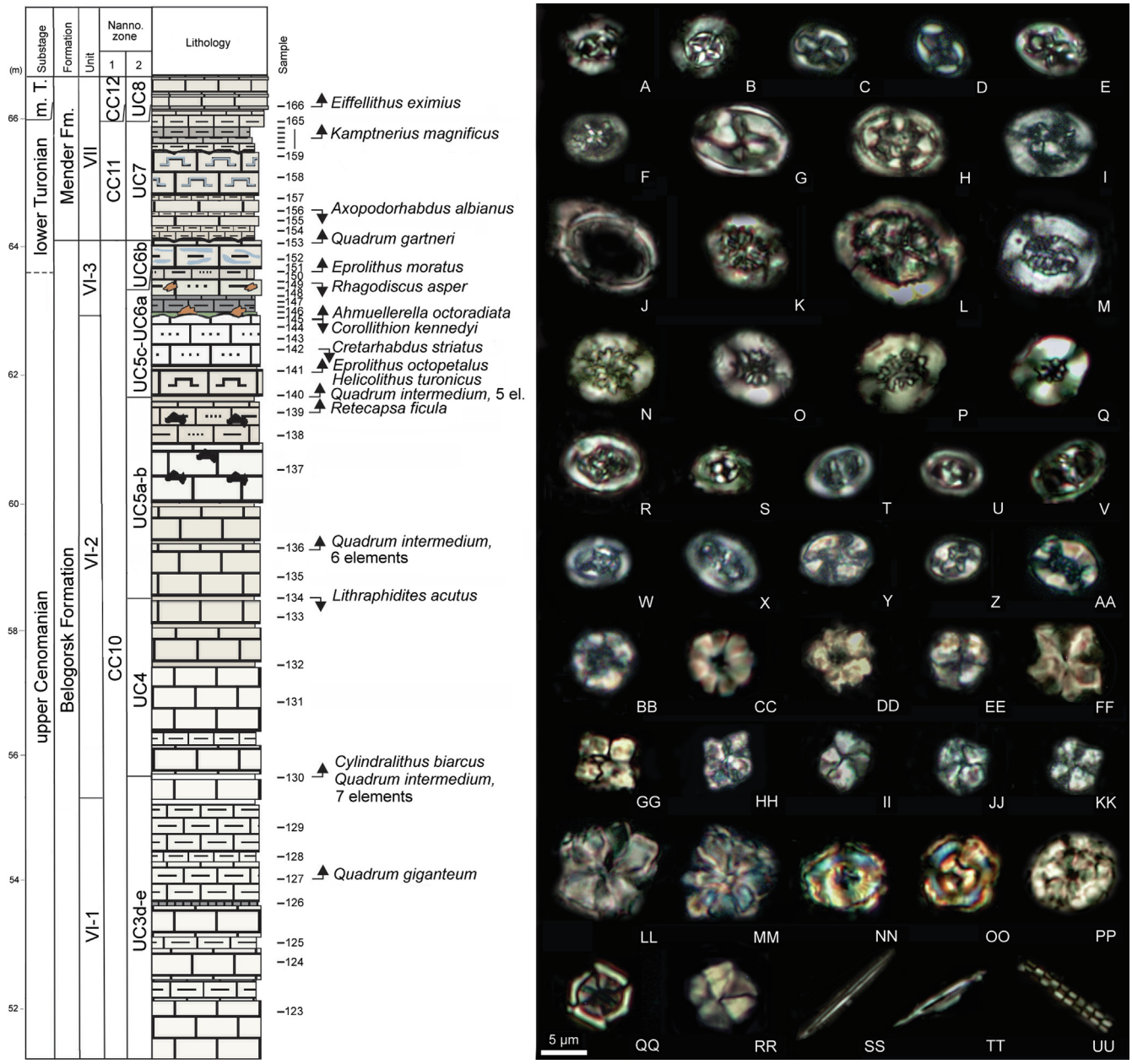

Fig. 5. Litho- and nannofossil stratigraphy of the upper Cenomanian to middle Turonian of Selbukhra section (outcrop 3 in Fig. 1B) and light microscope images of selected nannofossil species under cross polarization. Abbreviations: m. T – middle Turonian; el., elements. (A) *Prediscosphaera cretacea* (Arkhangelsky) Gartner, sample 162. (B) *P. columnata* (Stover) Perch-Nielsen, sample 150. (C) *Helicolithus compactus* (Bukry) Varol and Girgis, sample 152. (D) *H. turonicus* Varol and Girgis, sample 143. (E) *Chiastozygus litterarius* (Górka) Manivit, sample 132. (F) *Chiastozygus bifarius* Bukry, sample 157. (G) *Gartnerago segmentatum* (Stover) Thierstein, sample 159. (H) *Axopodorhabdus albianus* (Black) Wind and Wise, sample 124. (I) *Grantarhabdus coronadventis* (Reinhardt) Grün, sample 127. (J) *Kamptnerius magnificus* Deflandre, sample 159. (K) *Cretarhabdus conicus* Bramlette and Martini, sample 143. (L, M) *C. striatus* (Stradner) Black; (L) sample 130; (M) sample 138. (N) *Retecapsa schizobrachiata* (Gartner) Grün, sample 124. (O) *R. crenulata* (Bramlette and Martini) Grün in Grün and Allemann, sample 132. (P) *R. surirella* (Deflandre and Fert) Grün in Grün and Allemann, sample 126. (Q) *R. ficula* (Stover) Burnett, sample 138. (R) *Rhagodiscus asper* (Stradner) Reinhardt, sample 145. (S) *R. achlyostaurion* (Hill) Doeven, sample 164. (T) *Zeugrhabdotus diplogrammus* (Deflandre in Deflandre and Fert) Burnett, sample 132. (U) *Z. howei* Bown in Kennedy et al., sample 160. (V) *Z. scutula* (Bergen) Rutledge and Bown, sample 157. (W) *Z. trivectis* Bergen, sample 145. (X) *Staurolithites halfanii* Lees, sample 144. (Y) *Eiffellithus eximius* (Stover) Perch-Nielsen, sample 162. (Z) *E. perch-nielseniae* Shamrock, sample 123. (AA) *Eiffellithus* sp., sample 129. (BB) *Eprolithus apertior* Black, sample 165. (CC) *E. floralis* (Stradner) Stover, sample 137. (DD) *E. octopetalus* Varol, sample 143, 162. (EE) *E. moratus* (Stover) Burnett, sample 157. (FF) *Eprolithus* sp., sample 160. (GG) *Quadrum gartneri* Prins and Perch-Nielsen, sample 153. (HH) *Q. intermedium* Varol, 7 elements, sample 131. (II) *Q. intermedium* Varol, 6 elements, sample 136. (JJ) *Q. intermedium* Verol, 5 elements, sample 140. (KK) *Q. octobrachium* Varol, 162. (LL, MM) *Q. giganteum* Varol; (LL) sample 127; (MM) sample 162. (NN) *Cylindralithus nudus* Bukry, sample 132. (OO) *C. sculptus* Bukry, sample 136. (PP) *C. biarcus* Bukry, sample 137. (QQ) *Corollithion kennedyi* Crux, sample 138. (RR) *Braarudosphaera* cf. *hockwoldensis* Black, sample 123. (SS) *Lithraphidites carniolensis* Deflandre, sample 123. (TT) *L. acutus* Verbeek and Manivit, sample 134. (UU) *Microrhabdulus decoratus* Deflandre, sample 129.

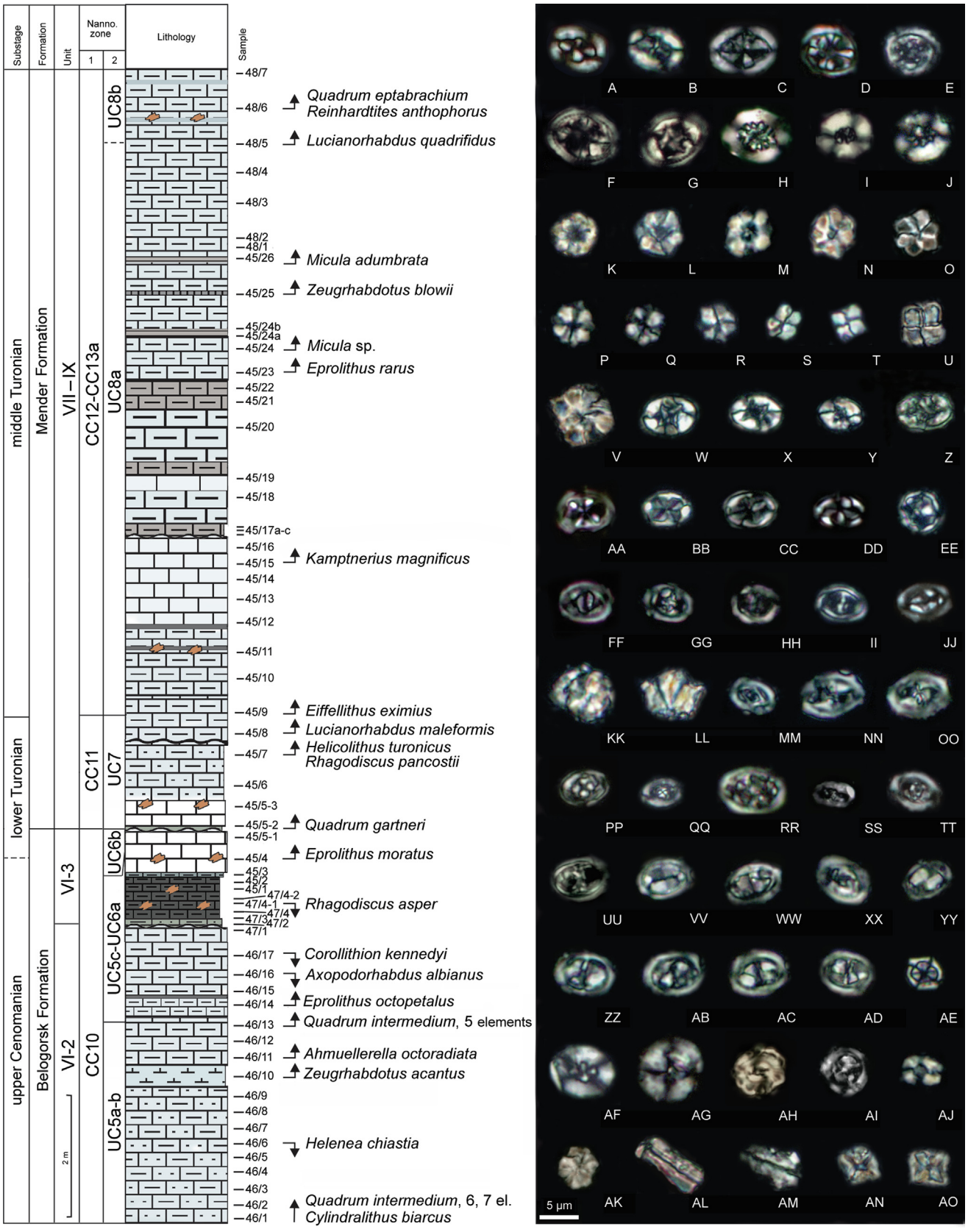
Substage
Formation
Unit
Nanno. zone
1
2
Lithology
Sample
middle Turonian
lower Turonian
upper Cenomanian
Mender Formation
Belogorsk Formation
VII–IX
VI-3
VI-2
CC12-CC13a
CC11
CC10
UC8b
UC8a
UC7
UC6b
UC5c-UC6a
UC5a-b
2 m
48/7
48/6
48/5
48/4
48/3
48/2
48/1
45/26
45/25
45/24b
45/24a
45/24
45/23
45/22
45/21
45/20
45/19
45/18
45/17a-c
45/16
45/15
45/14
45/13
45/12
45/11
45/10
45/9
45/8
45/7
45/6
45/5-3
45/5-2
45/5-1
45/4
45/3
45/2
45/1
47/4-2
47/4-1
47/4
47/3
47/2
47/1
46/17
46/16
46/15
46/14
46/13
46/12
46/11
46/10
46/9
46/8
46/7
46/6
46/5
46/4
46/3
46/2
46/1
Quadrum eptabrachium
Reinhardtites anthophorus
Lucianorhabdus quadrifidus
Micula adumbrata
Zeugrhabdotus blowii
Micula sp.
Eprolithus rarus
Kamptnerius magnificus
Eiffellithus eximius
Lucianorhabdus maleformis
Helicolithus turonicus
Rhagodiscus pancostii
Quadrum gartneri
Eprolithus moratus
Rhagodiscus asper
Corollithion kennedyi
Axopodorhabdus albianus
Eprolithus octopetalus
Quadrum intermedium, 5 elements
Ahmuellerella octoradiata
Zeugrhabdotus acantus
Helenea chiastia
Quadrum intermedium, 6, 7 el.
Cylindralithus biarcus
A B C D E
F G H I J
K L M N O
P Q R S T U
V W X Y Z
AA BB CC DD EE
FF GG HH II JJ
KK LL MM NN OO
PP QQ RR SS TT
UU VV WW XX YY
ZZ AB AC AD AE
AF AG AH AI AJ
AK AL AM AN AO
5 μm

of UC10 and CC14 zones roughly corresponding to the base of the middle Coniacian.

The occurrence of *Lithastrinus grilli*, *Lucianorhabdus cayeuxii*, *Micula concava*, *Rucinolithus hayi* and the absence of *Lithastrinus septenarius* at the base of the Unit XV indicate the interval of the middle–upper Santonian UC12 or undivided CC16-17 zones and define the range of stratigraphic hiatus as upper Coniacian to lower Santonian. The low-abundance nannofossil assemblage is characterized by wide occurrence of various large heavily calcified *Lucianorhabdus* spp. and *Calculites* spp. (Fig. 8LL–ZZ), which continues to be present up to the top of the studied part of the section. Small *Arkhangelskiella* (*A. confusa*), appeared at the Turonian/Coniacian transition at Aksudere section, progressively increases its size toward the top of Santonian (Fig. 8F–H) and specimens, which can be considered as typical (> 8 μm) *A. cymbiformis* (the marker of the base of UC13) are found at the level of sample 52/5. The LO of *Broinsonia parca parca* (a criterion for the bases of UC14 and CC18 zones) is observed in the upper part of Unit XV (sample 52/8).

The results of thorough study of the Santonian/Campanian transition at Aksudere section are given in Guzhikov et al., 2021. They established the base of Magnetochron C33r in the lower part of Unit XVI that falls into UC14 zone. This is in good accordance with the GSSP for the Campanian Stage in Botaccione section, Italy. However, this observation can be hardly correlated with our sampling, because the Santonian/Campanian transition was deeply buried in the year of our field work and we had no access to this part of section. *B. parca parca* shows progressive decrease of the diameter of central area toward the top of exposure and the specimens with the size of central area lower than rim (*B. parca constricta*, the marker of the base of UC14b subzone) are observed at the top of the studied succession (sample 53/4, Fig. 8E). Thus, the studied part of Aksudere section is surmounted with the early Campanian sediments.

4.2. Hiatuses and sequence boundaries

The detailed nannofossil zonation led to more precise definition of the stratigraphic range of hiatuses in the studied sedimentary record and sequence stratigraphic interpretation of the studied succession. According to Gale et al. (1999), two main supra-regional hiatuses, featured for the northern Tethyan margin, are identified in southwestern Crimea. The hiatus at the Albian/Cenomanian transition is estimated to be ranging the upper part of *Stoliczkaia dispar* and the whole *Mantelliceras mantelli* ammonite zones based on the occurrence of *Inoceramus virgatus* at 2 m above the erosional surface in the Cenomanian outcrop exposed in Kacha River basin (ca. 5 km southwest from Selbukhra section, close to Aksudere section). However, at Selbukhra section, the occurrence of nannofossil assemblage of the upper part of UC1 zone suggests shorter interval for this hiatus ranging the UC0 to lowermost UC1 zone (Figs. 2, 9) roughly correlatable with the lower part of *Neostlingoceras carcitanense* subzone (= lower part of *M. mantelli* zone, see Burnett, 1998). According to northwestern European sequence stratigraphy (compiled in Wilmsen et al., 2005; Wilmsen, 2012), the omitted interval at the base of Cenomanian at Selbukhra section likely corresponds to depositional sequence Ce I and the base of Cenomanian correlates to the sequence boundary (SB) Ce 1. Smooth hardground surface at the level ca. 8.3 m in the interval of undivided UC1d-UC2b subzones (Fig. 3) likely corresponds to the SB Ce 2 at the topmost *mantelli* zone (Hardenbol et al., 1998), which correlates with the upper part of UC1 nannofossil zone. The corresponding hiatus

Fig. 6. Litho- and nannofossil stratigraphy of the upper Cenomanian to middle Turonian of Aksudere section (outcrop 4 in Fig. 1B) and light microscope images of selected nannofossil species under cross polarization. (A) *Broinsonia enormis* (Shumenko) Manivit, sample 46/1. (B) *B. cenomanica* (Black) Bown, sample 46/6. (C) *Broinsonia* sp., sample 46/1. (D) *Ahmuellerella octoradiata* (Górka) Reinhardt, sample 46/13. (E) *Tetrapodorhabdus decorus* (Deflandre) Wind and Wise, sample 45/5.1. (F, G) *Axopodorhabdus albianus* (Black) Wind and Wise, sample 46/9. (H) *Retecapsa crenulata* (Bramlette and Martini) Grün, sample 46/3. (I) *R. ficula* (Stover) Burnett, sample 46/9. (J) *R. angustiforata* Black, sample 48/5. (K) *Eprolithus apertior* Black, sample 48/5. (L, M) *E. octopetalus* Varol; (L)sample 46/14; (M) sample 45/22. (N) *E. moratus* (Stover) Burnett, sample 45/3. (O) *E. rarus* Varol, sample 45/25. (P) *Quadrum eneabrachium* Varol, sample 46/16. (Q) *Q. octobrachium* Varol, sample 46/6. (R) *Q. eptabrachium* Varol, sample 48/6. (S) *Q. intermedium* Varol, sample 46/13. (T, U) *Q. gartneri* Prins and Perch-Nielsen; (T) sample 45/22; (U) sample 48/6. (V) *Q. giganteum* Varol, sample 48/1. (W) *Eiffellithus turriseiffelii* (Deflandre) Reinhardt, sample 46/12. (X) *E. perch-nielseniae* Shamrock, sample 45/8. (Y) *E. gorkae* Reinhardt, sample 46/12. (Z) *E. eximius* (Stover) Perch-Nielsen, sample 45/7. (AA) *Helicolithus anceps* (Górka) Noël, sample 46/3. (BB) *H. trabeculatus* (Górka) Verbeek, sample 46/9. (CC) *H. compactus* (Bukry) Varol and Girgis, sample 45/7. (DD) *H. turonicus* Varol and Girgis, sample 45/7. (EE) *Stoverius achylosus* (Stover) Perch-Nielsen, sample 45/10. (FF) *Zeugrhabdotus bicrescenticus* (Stover) Burnett, sample 46/1. (GG) *Z. howei* Bown, sample 46/14. (HH) *Z. blowii* Lees, sample 45/26. (II) *Z. acanthus* Reinhardt, sample 46/10. (JJ) *Z. clarus* Bown, sample 46/12. (KK, LL) *Z. kerguelenensis* Watkins; (KK) sample 46/14; (LL) sample 46/10, side view. (MM) *Zeugrhabdotus*? sp., sample 46/12. (NN, OO) *Reinhardtites*? sp., sample 46/10; (NN) rotated at 0°; (OO) rotated at 90. (PP) *Rhagodiscus achlyostaurion* (Hill) Doeven, sample 46/12. (QQ) *R. pancostii* Lees, sample 45/7. (RR) *R. asper* (Stradner) Reinhardt, sample 46/12. (SS) *R. gallagheri* Rutledge and Bown, sample 46/3. (TT) *R. sageri* Bown, sample 45/6. (UU) *Amphizygus brooksii* Bukry, sample 46/9. (VV) *Tranolithus orionatus* Reinhardt, sample 46/14. (WW) *T. minimus* (Bukry) Perch-Nielsen, sample 46/14. (XX) *Tranolithus bitraversus* (Stover) Bergen, sample 46/6. (YY) *Tranolithus* sp. 1, sample 46/6. (ZZ, AB) *Tranolithus* sp. 2, sample 46/10; (ZZ) rotated at 0°; (AB) rotated at 90°. (AC, AD) *Tranolithus* sp. 3, sample 46/14; (AC) rotated at 0°; (AD) rotated at 90°. (AE) *Corollithion kennedyi* Crux, sample 46/14. (AF) *Helenea chiastia* Worsley, sample 46/6. (AG) *Haqius circumradiatus* (Stover) Roth, sample 46/6. (AH) *Cylindralithus nudus* Bukry, sample 46/9. (AI) *C. biarcus* Bukry, sample 46/3. (AJ) *Munarinus lesliae* Risatti, sample 45/24. (AK) *Assipetra terebrodentarius* (Applegate et al.) Rutledge and Bergen, sample 45/6. (AL) *Lucianorhabdus quadrifidus* Forchheimer, sample 48/7. (AM) *L. maleformis* Reinhardt, sample 45/8. (AN) *Micula* sp. 1, sample 45/24. (AO) *Micula* sp. 2, sample 45/24.

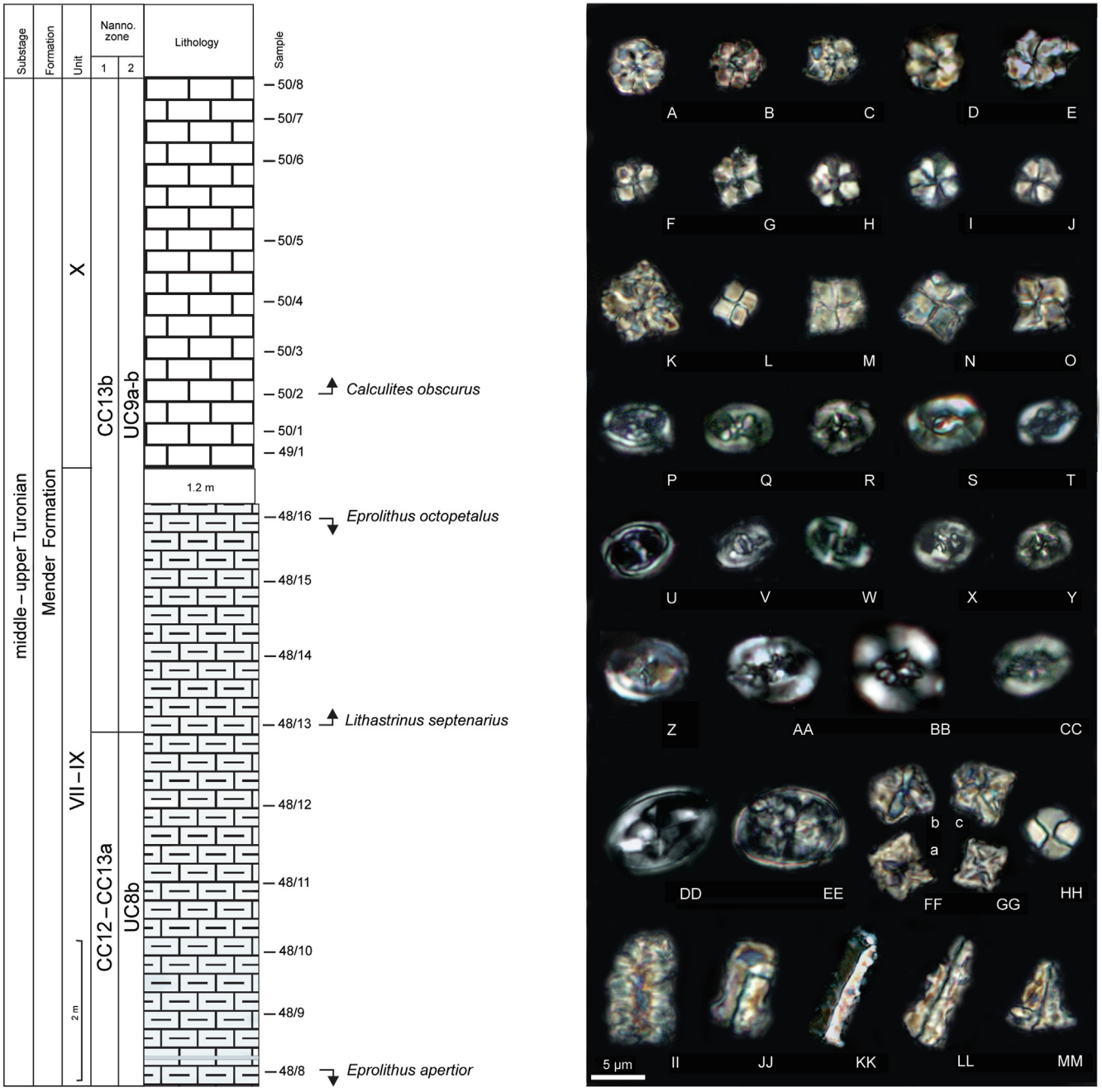

Fig. 7. Litho- and nannofossil stratigraphy of the middle–upper Turonian sediments of Aksudere section (outcrop 4 in Fig. 1B) and light microscope images of selected nannofossil species under cross polarization. (A) *Eprolithus octopetalus* Varol, sample 48/16. (B) *E. moratus* (Stover) Burnett, sample 48/11. (C) *E. rarus* Varol, sample 48/11. (D, E) *Lithastrinus septenarius* Forchheimer; (D) sample 48/13; (E) sample 50/8. (F) *Quadrum intermedium* Varol, sample 48/9. G) *Q. eneabrachium* Varol, sample 48/9. (H, I) *Q. octobrachium* Varol; (H) sample 48/11; (I) sample 48/16. (J) *Q. eptabrachium* Varol, sample 50/2. (K) *Q. giganteum* Varol, sample 50/6. (L–O) *Q. gartneri* Prins and Perch-Nielsen; (L) sample 48/16; (M) sample 48/16; (N) sample 50/1; (O) sample 50/6. (P) *Amphizygus brooksii* Bukry, sample 48/10. (Q) *Chiastozygus spissus* Bergen, sample 48/11. (R) *Staurolithites halfanii* Lees, sample 48/11. (S) *Biscutum dissimilis* Wind and Wise, sample 48/10. (T) *Broinsonia signata* (Noël), sample 50/6. (U) *Zeugrhabdotus acanthus* Reinhardt, sample 48/10. (V) *Z. bicrescenticus* (Stover) Burnett, sample 48/10. (W) *Z. blowii* Lees, sample 48/16. (X) *Z. howei* Bown, sample 50/1. (Y) *Zeugrhabdotus* sp., sample 50/1. (Z) *Reinhardtites* sp., sample 48/9. (AA) *Reinhardtites anthophorus* (Deflandre) Perch-Nielsen, sample 48/13. (BB) *Retecapsa octofenestrata* (Bralower) Bown, sample 48/12. (CC) *Sollasites horticus* (Stradner) Cepek and Hay, sample 48/16. (DD) *Gartnerago obliquum* (Stradner) Noël, sample 50/2. (EE) *Kamptnerius magnificus* Deflandre, sample 50/3. (FFa–c) *Micula* sp., sample 48/16; (a–c) are different specimens. (GG) *M. adumbrata* Burnett, sample 48/16. (HH) *Calculites obscurus* (Deflandre) Prins and Sissingh, sample 50/2. (II) *Nannoconus elongatus* Brönnimann, sample 48/9. (JJ, KK) *Lucianorhabdus quadrifidus* Forchheimer; (JJ) sample 50/3; (KK) sample 50/6. (LL, MM) *L. maleformis* Reinhardt; (LL) sample 50/2; (MM) sample 50/4.

more likely ranges very short interval at the *mantelli/dixoni* transition, including UC1/UC2 zonal boundary.

The clearly pronounced hardground at the top of the lower Cenomanian (the boundary between subunits IV-1

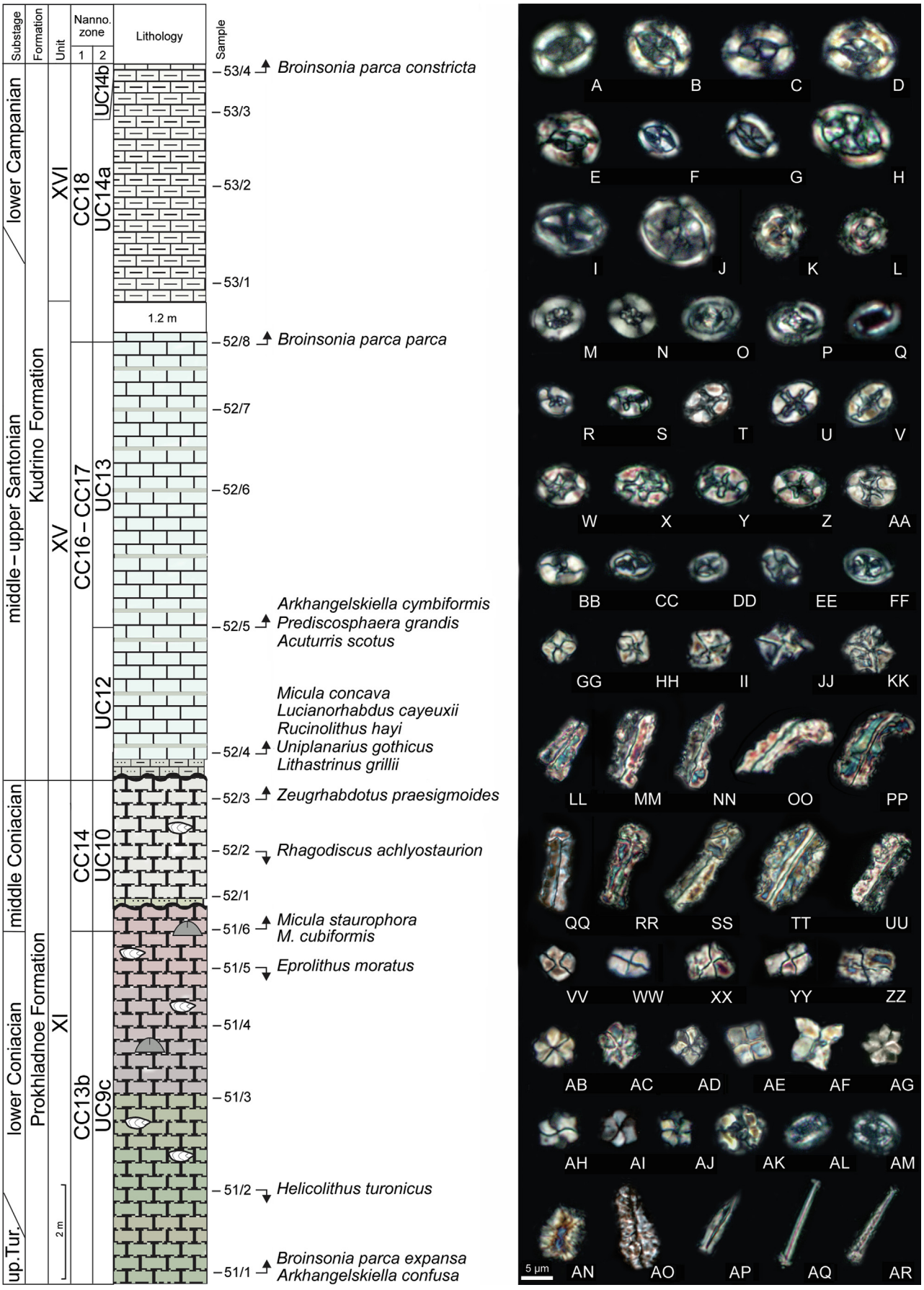
Substage
Formation
Unit
Nanno. zone
1
2
Lithology
Sample
lower Campanian
middle – upper Santonian
Kudrino Formation
Prokhladnoe Formation
lower Coniacian
middle Coniacian
up.Tur.
XVI
XV
XI
CC18
CC16 – CC17
CC14
CC13b
UC14b
UC14a
UC13
UC12
UC10
UC9c
1.2 m
2 m
53/4
53/3
53/2
53/1
52/8
52/7
52/6
52/5
52/4
52/3
52/2
52/1
51/6
51/5
51/4
51/3
51/2
51/1
Broinsonia parca constricta
Broinsonia parca parca
Arkhangelskiella cymbiformis
Prediscosphaera grandis
Acuturris scotus
Micula concava
Lucianorhabdus cayeuxii
Rucinolithus hayi
Uniplanarius gothicus
Lithastrinus grillii
Zeugrhabdotus praesigmoides
Rhagodiscus achlyostaurion
Micula staurophora
M. cubiformis
Eprolithus moratus
Helicolithus turonicus
Broinsonia parca expansa
Arkhangelskiella confusa
A B C D
E F G H
I J K L
M N O P Q
R S T U V
W X Y Z AA
BB CC DD EE FF
GG HH II JJ KK
LL MM NN OO PP
QQ RR SS TT UU
VV WW XX YY ZZ
AB AC AD AE AF AG
AH AI AJ AK AL AM
5 μm AN AO AP AQ AR

and IV-2) indicates the basal middle Cenomanian hiatus, which ranges the uppermost *dixonii* to lower part of *rhotomagense* ammonite zone as suggested by Gale et al. (1999) and corresponds to SB Ce 3. The interval of co-occurrence of *Lithraphidites acutus* and *Gartnerago theta* (UC3a subzone) correlates to the *inerme* ammonite zone and lowermost part of *rhotomagense* zone (Burnett, 1998). The occurrence of both species above the erosional surface (in the Subunit IV-2) suggests the hiatus ranging the uppermost *dixonii* to lower part of *inerme* ammonite zones (Fig. 9). The absence of *Lithraphidites acutus* from the poor in nannofossils basal part of Subunit IV-2 can signify its slightly later LO in Selbukhra section. Uncertainty in the position of the bases of UC3c and UC3d subzones does not allow the exact correlation with the ammonite zones. Possibly, these boundaries have lower position in the succession studied due to probable earlier disappearance of the marker species from the middle Cenomanian succession of Selbukhra section. This makes the stratigraphic range of UC3b subzone unlikely short, while actually this large subzone covers the interval of the most part of *rhotomagense*, *jukesbrowni* and the lower part of *guerangeri* zones. The 1.7 m thick limestone bed lying at the base of Unit VI (Fig. 5) likely represents HST and the upper surface of this bed correlates with the SB Ce 4 despite the absence of pronounced erosion. Above this boundary, the amount of siliciclastics decreases significantly (Alekseev et al., 2007). The SB Ce 5 corresponding to the base of *geslinianum* ammonite zone (≈ the base of UC4 nannofossil zone) falls into facies change from rhythmically thin-bedded marls and limestones to homogenous pale thick-bedded limestones with cherty concretions at the base of Subunit VI-2. The upper boundary of Subunit VI-2 represents hardground surface in both studied sections. The LO of *Ahmuellerella octoradiata*, which falls at the base of *juddii* ammonite zone (Burnett, 1998), is found in the topmost part of Subunit VI-2 at Selbukhra section that suggests a short hiatus corresponding to the upper part of *juddii* zone and, possibly, lowermost *devonense* zone. The small thickness of overlying lower Turonian UC6 and UC7 nannofossil zones indicates sediment condensation and erosion at the top of Selbukhra section and, in minor extent, in the lower part of Aksudere section (Figs. 5, 6). An erosional surface in the UC7 zone, better pronounced in Selbukhra section, corresponds to SB Tu 1 (*nodosoides* ammonite zone) of Hardenbol et al. (1998). Overlying sequence contains few thin dark clayey intercalations, possibly, marking indistinct short hiatuses. SB Tu 2 (*woollgari* ammonite zone and UC8a nannofossil subzone) falls into the hardground surface in the lower part of Mender Formation immediately above the LO of *Kamptnerius magnificus* (Figs. 2, 6). An unexposed interval at the base of Unit X covers the level of pronounced facies change, which possibly corresponds to the SB Tu 3 (the base of *deverianum* ammonite subzone and lower UC9 nannofossil zone). The SB Tu 4 (upper part of *neptuni* ammonite zone and UC9b nannofossil subzone) more likely falls to the covered interval at the base of Unit XI (Prokhladnoe Formation) corresponding to significant facial changes (Figs. 2, 9).

Short hiatus within the middle Coniacian UC10 (CC14) likely corresponds to the eustatic sea-level fall in the *tridorsatum* ammonite zone denoted as sequence boundary KCo 1 (Haq, 2014). The major stratigraphic hiatus at the Coniacian/Santonian transition ranges the upper part of UC10 zone to lower part of UC12 zone and more likely coincides with the SB KSa 2 in the *gallicus* ammonite zone (Haq, 2014).

Fig. 8. Litho- and nannofossil stratigraphy of the upper Turonian to lower Campanian of Aksudere section (outcrop 5 in Fig. 1B) and light microscope images of selected nannofossil species under cross polarization. Abbreviation: up. Tur., upper Turonian. (A, B) *Broinsonia parca expansa* Wise and Watkins; (A) sample 52/3; (B) sample 53/1. (C, D) *Broinsonia parca parca* (Stradner) Bukry; (C) sample 52/8; (D) sample 53/4. (E) *Broinsonia parca constricta* Hattner et al., sample 53/4. (F) *Arkhangelskiella confusa* Burnett, sample 51/1. (G, H) *Arkhangelskiella cymbiformis* Vekshina; (G) sample 52/5; (H) sample 53/4. (I) *Gartnerago segmentatum* (Stover) Thierstein, sample 51/1. (J) *Kamptnerius magnificus* Deflandre, sample 51/1. (K) *Cylindralithus biarcus* Bukry, sample 52/5. (L) *C. sculptus* Bukry, sample 52/6. (M) *Retecapsa crenulata* (Bramlette and Martini) Grün, sample 52/3. (N) *Retecapsa octofenestrata* (Bralower) Bown, sample 52/3. (O, P) *Reinhardtites anthophorus* (Deflandre) Perch-Nielsen; (O) sample 52/3; (P) sample 52/5. (Q) *Biscutum magnum* Wind and Wise, sample 53/3. (R, S) *Eiffellithus gorkae* Reinhardt; (R) sample 52/5; (S) sample 52/8. (T–Z) *E. eximius* (Stover) Perch-Nielsen; (T) sample 51/6; (U) sample 52/2; (V) sample 52/4; (W) sample 52/5; (X, Y) sample 52/6; (Z) sample 53/4. (AA) *E. digitatus* Shamrock, sample 52/3. (BB) *E. lindiensis* Lees, sample 52/3. (CC) *Zeugrhabdotus praesigmoides* Burnett, sample 52/3. (DD) *Staurolithites flavus* Burnett, sample 52/3. (EE) *Helicolithus turonicus* Varol and Girgis, sample 51/1. (FF) *H. anceps* (Górka) Noël, sample 52/4. (GG) *Micula staurophora* (Gardet) Stradner, sample 51/6. (HH) *M. cubiformis* Forchheimer, sample 52/3. (II–KK) *M. concava* (Stradner) Verbeek; (II) sample 52/5; (JJ) sample 52/8; (KK) sample 53/3. (LL, MM) *Lucianorhabdus maleformis* Reinhardt; (LL) sample 52/3; (MM) sample 52/6. (NN–PP) *Lucianorhabdus cayeuxii* Deflandre; (NN) sample 52/3; (OO) sample 52/5; (PP) sample 52/6. (QQ, RR) *L. quadrifidus* Forchheimer; (Q) sample 52/6; (RR) sample 53/2. (SS) *Lucianorhabdus*? *cubiterminalis* Farhan et al., sample 52/3. (TT, UU) *L. windii* Hattner and Wise; (TT) sample 52/3; (UU) sample 52/8. (VV) *Calculites obscurus* (Deflandre) Prins and Sissingh, sample 52/3. (WW) *C. ovalis* (Stradner) Prins, sample 52/8. (XX–ZZ) *Calculites* sp.; (XX) sample 52/6; (YY, ZZ) sample 52/8. (AB) *Eprolithus floralis* (Stradner) Stover, sample 51/1. (AC) *E. rarus* Varol, sample 52/6. (AD) *Quadrum intermedium* Varol, sample 51/1. (AE) large *Q. gartneri* Prins and Perch-Nielsen, possibly transitional form to *Uniplanarius*, sample 51/1. (AF) *Uniplanarius gothicus* (Deflandre) Hattner and Wise, sample 53-1. (AG) *Lithastrinus septenarius* Forchheimer, sample 51/5. (AH) *L. grillii* Stradner, sample 52/4. (AI) *Hexalithus gardetiae* Bukry, sample 52/4. (AJ) *Rucinolithus hayi* Stover sample 53/1. (AK) *Cribrocorona gallica* (Stradner) Perch-Nielsen, sample 52/8. (AL) *Cribrosphaerella ehrenbergii* (Arkhangelsky) Deflandre, sample 53/3. (AM) *C. pelta* Gartner, sample 52/8. (AN) *Nannoconus truittii frequens* Deres and Achéritéguy, sample 51/4. (AO) *Nannoconus elongatus* Brönnimann, sample 51/1. (AP) *Acuturris scotus* (Risatti) Wind and Wise, sample 52/5. (AQ, AR) *Zeugrhabdotus* spikes?, sample 52/8.

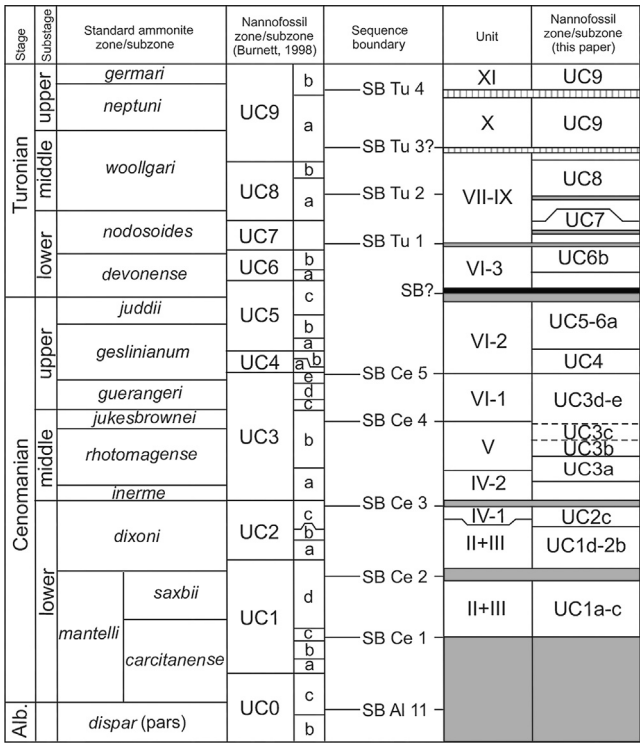

Fig. 9. Cenomanian to Turonian biostratigraphy, global sequence boundaries and hiatuses recognized in Selbukhra and Aksudere sections. Fine lines – facial changes and short hiatuses at the unit and subunit boundaries; perpendicular hatching – possible hiatuses; grey – hiatuses with pronounced erosion; thick black line – Bonarelli Level (OAE 2). Abbreviation: Alb., Albian.

5. Discussion

5.1. Biostratigraphy

The high-resolution study of nannofossils from the upper Cenomanian to lowermost Campanian succession of southwestern Crimea revealed a series of the most important nannofossil zonal/subzonal markers and showed the potential for use of the standard Upper Cretaceous zonations of Sissingh (1977) refined by Perch-Nielsen (1985) and Burnett (1998). The most part of stratigraphic markers display their lower and high occurrences coeval to the levels used in these zonations. At the same time, some species appeared to be unreliable markers for this area. For example, the HO of *Corollithion kennedyi* denotes the base of UC3e subzone in the Burnett' zonation. At Selbukhra and Aksudere sections, this species occurs up to the top of UC5 (Fig. 10), showing its HO immediately below the black shale of OAE2. The later HO of *C. kennedyi* at the similar level is shown in many areas: Dolomites, Italy (Luciani and Cobianchi, 1999), Upper Austria (Wagreich et al., 2008), Germany (Linnert et al., 2010), Vocontian Basin, southeastern France (Fernando et al., 2010), Texas, USA (Lowery et al., 2014; Denne et al., 2016). Similarly, the HO of *Cretarhabdus striatus*, marking the base of UC4b subzone, is found at the top of UC5 at Selbukhra section. Such enlarged stratigraphic range of this species is not unique: the late LO of *Cretarhabdus striatus* (in the lowermost Turonian) is recorded in Romania (Melinte-Dobrinescu and Bojar, 2008) and Arobes section, Spain (Melinte-Dobrinescu et al., 2013).

The suggestion about the late LO of *Cylindralithus biarcus* (the base of UC4 zone) can be supported by the occurrence of relatively poor nannofossil assemblage enriched in cool-water *Eprolithus* in the upper part of the interval assigned to UC3d-e subzones at Selbukhra section. A decline in nannofossil productivity is reported from the *Plenus* marl (Lamolda et al., 1994) correlatable with UC4 zone. The HO of *Axopodorhabdus albianus* defines the base of UC5b. At Aksudere section, this species has its HO ca. 1.0 m below the OAE2. However, at Selbukhra section, it was found above the LO of *Quadrum gartneri* (the base of the lower Turonian UC7 zone). The same level of *A. albianus* disappearance is reported from the Western Interior Seaway (Bralower, 1988), Eastern Carpathians (Cetean et al., 2008), eastern Germany (Linnert et al., 2010). Obviously, the wider stratigraphic range of some upper Cenomanian stratigraphic markers can be the result of sediment redeposition. However, the regularity in their later occurrences in different areas should be taken into consideration.

Another nannofossil species, *Quadrum intermedium*, shows unusually early LO. The first specimens of *Quadrum* cf. *intermedium* appear in the lower part of Unit V (UC3a subzone). Typical *Q. intermedium* with 8 wall-cycle elements is found in UC3b subzone and further evolution of this species shows a trend to successive reduce of the number of elements up to five. The early LO of *Q. intermedium* in *geslinianum* ammonite zone is reported by Desmare et al. (2020) from the Cenomanian stratotype area. The LO of *Q. intermedium* with 5 elements falls into the middle *Neocardioceras juddii* ammonite zone and represents a reliable bioevent for the recognition of the uppermost Cenomanian UC5c subzone in Crimea.

Unit VI was traditionally considered in Crimea as the upper Cenomanian (Alekseev, 1989), although these sediments are very poor in macrofossils. However, Gale et al. (1999) reported two levels of *Amphidonte* bivalve concentration in the lower part of this Unit and, thus, this interval was suggested to be corresponding to the upper *jukesbrownei*–lower *guerangeri* ammonite zone, i.e., close to the base of the upper Cenomanian. Therefore, the boundary between the middle and upper Cenomanian, defined as the base of *guerangeri* zone, falls in the lower part of Unit VI. This conclusion cannot be unequivocally supported by the results of nannofossil study. All nannofossil bioevents (HOs of *Staurolithites gausorhethium*, *Gartnerago nanum* and *Corollithion kennedyi*) correlating with the interval of *guerangeri* zone (Fig. 9) are inconsistent at Selbukhra section because of the scarcity of first two species in the section and later LO of the last one. The LO of *Cylindralithus biarcus*, which is considered to be close above the base of the upper Cenomanian *geslinianum* ammonite zone

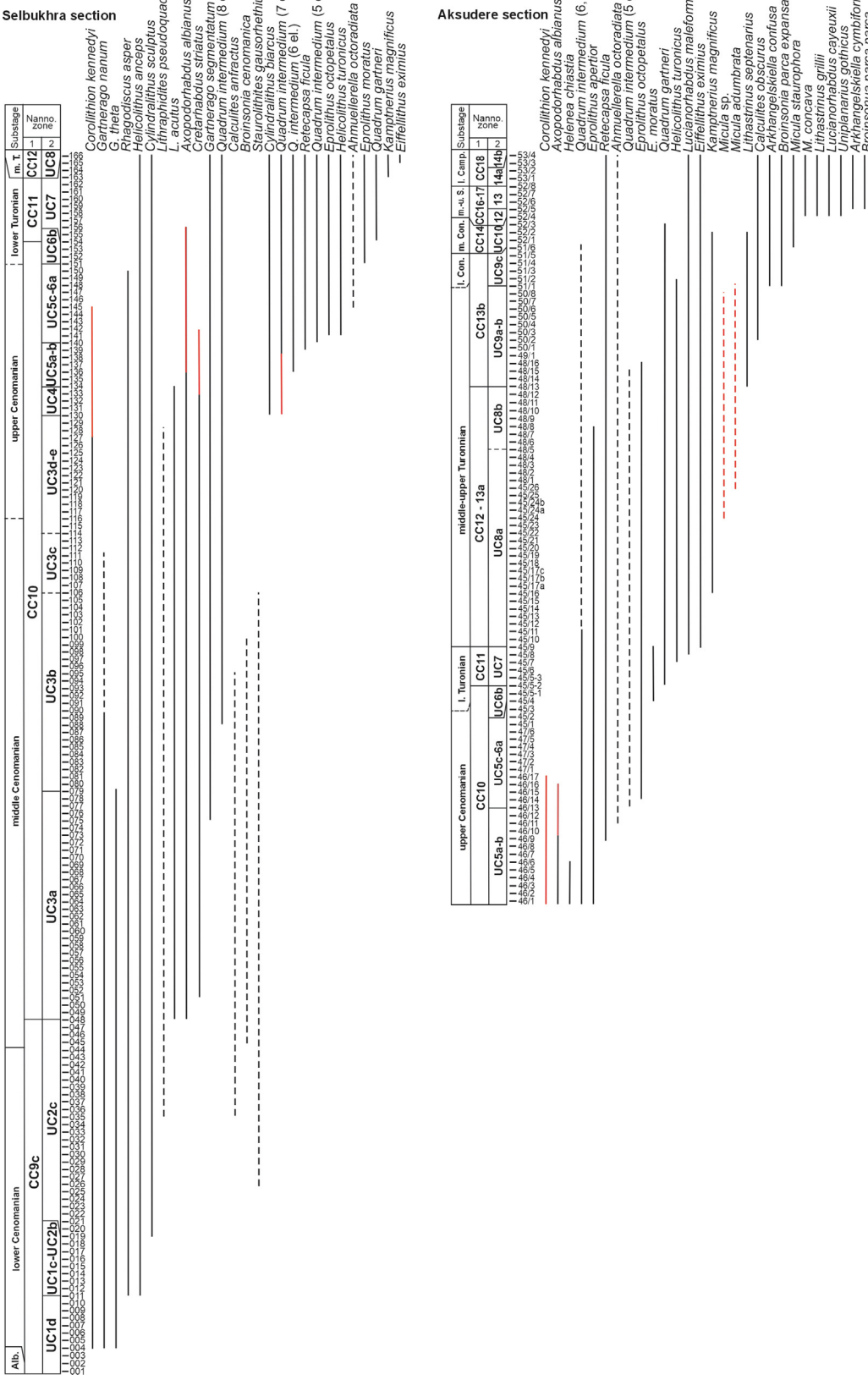

Fig. 10. Stratigraphic range of selected nannofossil species in the Selbukhra and Aksudere sections. Sporadic occurrence is shown in dashed line, expanded stratigraphic range of some species is shown in red line. Note the substages and nannofossil zones are shown in terms of their thickness in the studied sections. Abbreviations: l. Turonian – lower Turonian, m. T. – middle Turonian, l. Con. – lower Coniacian, m. Con. – middle Coniacian, m. – u. S. – middle–upper Santonian, l. Camp. – lower Campanian, el. – elements.

(Burnett, 1998), is found at the base of Subunit VI-1. The low diverse nannofossil assemblage and increased abundance of the cool-water *Eprolithus* spp. in the sediments of the topmost UC3 zone and almost the whole UC4 zone is likely caused by the relative climatic cooling known as Plenus Cold Event (PCE) (Gale and Christensen, 1996; Jarvis et al., 2011; O'Connor et al., 2020).

Specific low-diverse, taxonomically poor and *Watznaueria*-dominated nannofossil assemblage of Bonarelli Level is characterized by small-sized specimens that can be interpreted differently. A series of the recent morphometric research suggested environmental variations caused the formation of small-sized coccoliths such as increased nutrient availability (Lees et al., 2005), instable environment (Giraud, 2009), cooling (Bornemann and Mutterlose, 2006) and surface water acidification (Bottini and Faucher, 2020). Whatever the causes of nannofossil impoverishment and dwarfism are, this signalizes hostile environment during black shale accumulation. Our interpretation of environmental changes occurred during OAE2 and minor Cenomanian to Turonian palaeoecological events will be given in the upcoming special paper.

The scarcity of *Helenea chiastia* in Crimea and its inconsistent HO level make the usability of this species as zonal marker questionable in this area, while the LO of *Eprolithus moratus* seems to be trustworthy marker for the lower Turonian. Small thickness of the lower Turonian sediments in the studied area is caused by two short hiatuses at the base and in the middle of UC7 (CC11) nannofossil zone. The very early LO of *Micula* sp. and *M. adumbrata* in the middle Turonian of Aksudere section (Fig. 6) seems to be typical for northeastern Peri-Tethys, because they were observed at the similar level in the northeastern Caucasus (E. Shcherbinina personal observations). Besides, Roth and Bowdler (1979) indicated the first occurrence of *Micula* in the middle Turonian.

The upper part of Turonian is characterized by the beginning of progressive reduce of *Watznaueria* abundance (Table S8), which widely dominated nannofossil assemblage during the early Cretaceous to early Turonian. This trend was slightly weakened in the Coniacian and continued in the Santonian and Campanian. In the Coniacian and, especially, Santonian, the important part of nannofossil assemblage is played by diverse *Lucianorhabdus*, *Micula* and *Arkhangelskiellaceae*, while *Quadrum* became eliminated. This turnover in nannofossil assemblage was shown by Burnett (1998). Melinte and Lamolda (2007) and Lamolda et al. (2014) reported increased abundance of *Lucianorhabdus* spp., *Calculites* sp. and *Micula concava* at the base of Santonian in Spain and Romania. At Aksudere section, the last two taxa are rare in Santonian, but became more abundant in the Campanian. *Lucianorhabdus*, *Micula* and *Arkhangelskiellaceae* are mostly high-latitude taxa (Bukry, 1973; Wind, 1979; Lees, 2007; etc.), and their bloom in Santonian is likely related to the continuous cooling of Crimean basin.

5.2. Sequence stratigraphy

The architecture of the Cenomanian to Turonian sediments of Crimea is similar to the cyclically built pelagic sedimentary successions of the Dolomite basin, containing multiple black shale intercalations in the middle Cenomanian and at the Bonarelli Level (Luciani and Cobianchi, 1999), Vocontian basin in southeastern France (Gyawali et al., 2017) and northeastern Caucasus (Gavrilov and Shcherbinina, unpublished data). This suggests environmental resemblance of sedimentary regimes in the western and eastern margins of Tethyan Ocean at this time span. Occurrence of a number of hiatuses in the sedimentary record of Crimean basin indicates shallower depth of sediment accumulation in this part of Peri-Tethyan basin. Detailed nannofossil stratigraphy allowed the correlation of the Crimean Cenomanian to Turonian sediments with the sedimentary successions of Boreal realm, divided on the basis of ammonite stratigraphy (Wilmsen and Voigt, 2006; Wilmsen, 2007). This revealed a coevality of the main hiatuses and facial changes in the Cenomanian to Turonian lithological record from Crimea to European sequence boundaries (Hardenbol et al., 1998). Thus, the hardground at the base of Cenomanian exposed at Selbukhra section corresponds to the hardground and the sequence boundary identified just below the base of *saxbii* subzone (the upper part of *mantelli* zone) at Lüneburg section, Germany (Wilmsen et al., 2021) and Boulonnais, northwestern France (Robaszynski et al., 1998). In the North Cantabrian Basin, northern Spain, this level coincides with prominent facies change from siliciclastic to carbonate (Wiese and Wilmsen, 1999). The hardground surface at the base of middle Cenomanian (SB Ce 3) corresponding to the dramatic sea-level fall is observed at the base of Subunit IV-2 at Selbukhra section, in Germany and Anglo-Paris Basin (Robaszynski et al., 1998; Wilmsen, 2007), Vocontian Basin, southeastern France (Reboulet et al., 2013) and North Cantabrian Basin (Wiese and Wilmsen, 1999). The SB Ce 5 is known as 'sub-*plenus* erosion' in the Anglo-Paris Basin (Gale and Christensen, 1996; Robaszynski et al., 1998; Gale et al., 2005) and Germany (Voigt et al., 2006; Wilmsen and Voigt, 2006; Wiese et al., 2009). Although no prominent erosion is observed in Selbukhra section, this level corresponds to the facies change between subunits VI-1and VI-2. The erosional surface at the base of Subunit VI-3 is not labeled as SB in the classical chart of Hardenbol et al. (1998), but corresponds to SB KTu1 of Haq (2014) and hardgrounds at this level are referred from many World' areas: Western Interior Basin (Gale et al., 2008), North Cantabrian Basin (Wiese and Wilmsen, 1999), Anglo-Paris Basin and Cauvery Basin (Gale et al., 2002), Egypt (Farouk, 2015), etc. Pronounced erosional surface below the black shale of Bonarelli Level is observed in the many sections of the wide area of northeastern Peri-Tethys (Gavrilov et al., 2022) and represents the peculiarity of sedimentary regime in the Crimea-Caucasus basin at the Cenomanian/Turonian transition.

The multiple short hiatuses at the lower Turonian, more likely, reflect regional tectonics and/or hydrodynamics and suggest significant shallowing of the basin. Similar sediment architecture is observed in the northeastern Caucasus (Gavrilov and Shcherbinina, unpublished data). The transition between units IX and X falls into interval between outcrops 4 and 5, where the major facies change from soft white limestones to compact green limestones with stylolites. Although this interval was not cropped-out during our field works, Alekseev (1989) refers the erosion and redeposition at the base of Unit X. More likely, this level corresponds to the mid-Turonian hardground and disconformity referred to from the western Tethys (Gale, 2019).

A wide stratigaphic range of the post-Turonian hiatuses in Crimea is believed to be caused by regional tectonic events (Nikishin et al., 2015) leading to the omission of the lower part of middle Coniacian and the upper Coniacian to lower middle Santonian sediments. At the same time, both hiatuses corresponds to the major eustatic sea-level falls (Haq, 2014). Occurrence of large urchins and inoceramids and low nannofossil diversity suggests relatively low water depths in Crimean basin in Coniacian followed by deepening during the Santonian to early Campanian.

6. Conclusions

The intermediate palaeogeographic position of the shelf of the Crimean basin between Tethyan and Boreal realms drove the high taxonomical diversity of calcareous nannoplankton assemblages in the Late Cretaceous. The detailed study of nannofossil distribution in the most complete succession of southwestern Crimea has refined the stratigraphic range of the main lithological bodies (formations and units) and hiatuses in the Cenomanian to lower Campanian sedimentary record. The identification of the standard nannofossil zones in the northeastern Peri-Tethys is important for the correlation to the Tethyan and Boreal Upper Cretaceous and timing of geological and palaeoclimatic events in the basin. A series of earlier lowest and later highest occurrences of some nannofossil species recognized in the studied successions can shed some lights on the nannofossil evolution and palaeobiogeography. The biostratigraphic study enabled the correlation of the main hiatuses and the levels of facial changes to the European sequence stratigraphic events. This provides an additional tool for inter-basin correlation of the Upper Cretaceous sediments and demonstrates integrity of the Cretaceous evolution of northeastern Peri-Tethys with the western Tethyan margin.

Acknowledgements

This work was supported by the funds of the Geological Institute of the Russian Academy of Sciences. We thank Dr. Shi-Jun Jiang and two anonymous reviewers of this paper for careful reading of the manuscript and very helpful remarks and comments.

Supplementary data

Supplementary data to this article can be found online at https://doi.org/10.1016/j.palwor.2024.11.010.

References

Alekseev, A.S., 1989. Cretaceous System. Upper Series. In: Mazarovich, O.A., Mileev, V.S. (Eds.), Geological Structure of the Kacha Height of the Mountainous Crimea 1, Mesozoic Stratigraphy. Moscow State University Press, Moscow, pp. 123–149 (in Russian).

Alekseev, A.S., Kopaevich, L.F., Nikishin, A.M., Kuzmicheva, T.A., Ovechkina, M.N., 2007. Cenomanian–Turonian boundary sediments from the southwestern Crimea. Bulletin of the Moscow Naturalist Society, Geological Section 82 (3), 3–29 (in Russian).

Baraboshkin, E.Yu., Zibrov, I.A., 2012. Characteristics of the middle Cenomanian rhythmic succession of Selbukhra Mt. (southwestern Crimea). Moscow University Bulletin. Series 4. Geology 3, 35–42 (in Russian).

Benyamovsky, V.N., Kopaevich, L.F., 2016. Coniacian–Campanian Alan-Kyr section of the Mountainous Crimea: biostratigraphy and palaeobiogeography. Moscow University Bulletin. Series 4. Geology 2, 3–17 (in Russian).

Bornemann, A., Mutterlose, J., 2006. Size analyses of the coccolith species *Biscutum constans* and *Watznaueria barnesiae* from the Late Albian "Niveau Breistroffer" (SE France): taxonomic and palaeoecological implications. Geobios 39 (5), 599–615.

Bottini, C., Faucher, G., 2020. *Biscutum constans* coccolith size patterns across the mid Cretaceous in the western Tethys: Paleoecological implications. Palaeogeography, Palaeoclimatology, Palaeoecology 555, 109852.

Bown, P.R., Young, J.R., 1998. Techniques. In: Bown, P.R. (Ed.), Calcareous Nannofossil Biostratigraphy, British Micropalaeontological Society Publications Series. Chapman and Kluwer Academic Publishers, London, pp. 16–28.

Bragina, L.G., 1999. Cenomanian to Turonian radiolarians of the Mountain Crimea. Bulletin of the Moscow Naturalist Society, Geological Section 74 (3), 43–50 (in Russian).

Bralower, T.J., 1988. Calcareous nannofossil biostratigraphy and assemblages of the Cenomanian–Turonian boundary interval: implications for the origin and timing of oceanic anoxia. Paleoceanography 3, 275–316.

Bukry, D., 1973. Coccolith and silicoflagellate stratigraphy, Tasman Sea and Southwestern Pacific Ocean, Deep Sea Drilling Project Leg 21. In: Burns, R.E., Andrew, J.E., van der Lingen, G.J., Churkin, M., Galehouse, J.S., Packham, G.H., Davies, T.A., Kennett, J.P., Dumitrica, P., Edwards, A.R., Von Herzen, R.P. (Eds.), Initial Reports of the Deep Sea Drilling Project 21. U.S. Government Printing Office, Washington, pp. 885–893.

Burnett, J.A., 1998. Upper Cretaceous. In: Bown, P.R. (Ed.), Calcareous Nannofossil Biostratigraphy, British Micropalaeontological Society Publications Series. Chapman and Kluwer Academic Publishers, London, pp. 132–199.

Cetean, C.G., Bălc, R., Kaminski, M.A., Filipescu, S., 2008. Biostratigraphy of the Cenomanian–Turonian boundary in the Eastern Carpathians (Dâmboviţa Valley): preliminary observations. Studia Universitatis Babeş-Bolyai, Geologia 53 (1), 11–23.

Denne, R., Breyer, L., Callender, A., Hinote, R., Kariminia, M., Kosanke, T., Kita, Z., Lees, J., Rowe, H., Spaw, J., Tur, N., 2016. Biostratigraphic and geochemical constraints on the stratigraphy and depositional environments of the Eagle Ford and Woodbine Groups of Texas. In: Breyer, J.A. (Ed.), The Eagle Ford Shale: A Renaissance in U.S. Oil Production. AAPG Memoir 110, 1–86.

Desmares, D., Testé, M., Broche, B., Tremblin, M., Gardin, S., Villier, L., Masure, E., Grosheny, D., Morel, N., Raboeuf, P., 2020. High-resolution biostratigraphy and chemostratigraphy of the Cenomanian stratotype area (Le Mans, France). Cretaceous Research 106, 104198.

Dolitskaya, I.V., 1972. Peculiarities of the foraminifera facial affinity in the upper Cretaceous sediments of the Mountain Crimea. Izvestia Akademii Nauk SSSR, Geological Series 4, 123–135 (in Russian).

Farouk, S., 2015. Upper Cretaceous sequence stratigraphy of the Galala Plateaux, western side of the Gulf of Suez, Egypt. Marine and Petroleum Geology 60 (3), 136–158.

Fernando, A.G.S., Takashima, R., Nishi, H., Giraud, F., Okada, H., 2010. Calcareous nannofossil biostratigraphy of the Thomel Level (OAE2) in the Lambruisse section, Vocontian Basin, southeast France. Geobios 43 (1), 45–57.

Gabdullin, R.R., 2002. Rhythmicity of the Upper Cretaceous Sediments of Russian Plate, Northeastern Caucasus and Southwestern Crimea (Structure, Classification, Models of Formation). Moscow State University Press, Moscow, 304 pp. (in Russian).

Gale, A.S., 2019. Correlation, age and significance of Turonian Chalk hardgrounds in southern England and northern France: The roles of tectonics, eustasy, erosion and condensation. Cretaceous Research 103, 104164.

Gale, A.S., Christensen, W.K., 1996. Occurrence of the belemnite *Actinocamax plenus* in the Cenomanian of SE France and its significance. Bulletin of the Geological Society of Denmark 43, 68–77.

Gale, A.S., Hancock, J.M., Kennedy, W.J., 1999. Biostratigraphical and sequence correlation of the Cenomanian successions in Mangyshlak (W. Kazakhstan), Crimea (Ukraine) with those in southern England. Bulletin de l'Institut Royal des Sciences Naturelles de Belgique, Sciences de la Terre 69, 67–86.

Gale, A.S., Hardenbol, J., Hathaway, B., Kennedy, W.J., Young, J.R., Phansalkar, V., 2002. Global correlation of Cenomanian (Upper Cretaceous) sequences: Evidence for Milankovitch control on sea level. Geology 30 (4), 291–294.

Gale, A.S., Voigt, S., Kennedy, W.J., Walaszczyk, I., 2005. Stratigraphy of the Upper Cenomanian–Lower Turonian Chalk succession at Eastbourne, Sussex, UK: ammonites, inoceramid bivalves and stable carbon isotopes. Cretaceous Research 26, 460–487.

Gale, A.S., Voigt, S., Sageman, B.B., Kennedy, W.J., 2008. Eustatic sea-level record for the Cenomanian (Late Cretaceous) — Extension to the Western Interior Basin, USA. Geology 36 (11), 859–862.

Gavrilov, Yu.O., Shcherbinina, E.A., Shchepetova, E.V., Golovanova, O. V., Pokrovsky, B.G., 2022. Late Cenomanian Paleoecological Event OAE 2 in the sections of the northern Peri-Tethys (Crimea, Eastern Caucasus): Sediment structure and dynamics of their accumulation. Lithology and Mineral Resources 57 (6), 473–493.

Giraud, F., 2009. Calcareous nannofossil productivity and carbonate production across the Middle–Late Jurassic transition in the French Subalpine Basin. Geobios 42, 699–714.

Guzhikov, A.Y., Baraboshkin, E.Y., Aleksandrova, G.N., Ryabov, I.P., Ustinova, M.A., Kopaevich, L.F., Mirantsev, G.V., Kuznetsov, A.B., Fokin, P.A., Kosorukov, V.L., 2021. New bio-, chemo-, and magnetostratigraphy of the Santonian–Campanian boundary in the Kudrino and Aksu-Dere sections (SW Crimea): Problems of global correlation and selection of the lower boundary stratotype of the Campanian. 1. Geological framework, sedimentology, biostratigraphy. Stratigraphy and Geological Correlation 29, 450–494.

Gyawali, B.R., Nishi, H., Takashima, R., Herrle, J.O., Takayanagi, H., Latil, J.-L., Iryu, Y., 2017. Upper Albian–upper Turonian calcareous nannofossil biostratigraphy and chemostratigraphy in the Vocontian Basin, southeastern France. Newsletters on Stratigraphy 50, 111–139.

Haq, B.U., 2014. Cretaceous eustasy revisited. Global and Planetary Change 113, 44–58.

Hardenbol, J., Thierry, J., Farley, M.B., Jaquin, T., Graciansky, P.-C., Vail, P.R., 1998. Mesozoic and Cenozoic sequence stratigraphy of European basins. SEPM Special Publication 60, 3–13.

Jarvis, I., Lignum, J.S., Gröcke, D.R., Jenkyns, H.C., Pearce, M.A., 2011. Black shale deposition, atmospheric CO_2 drawdown, and cooling during the Cenomanian–Turonian Oceanic Anoxic Event. Paleoceanography 26, PA3201.

Kalinichenko, G.P., 1983. Calcareous nannofossils and zonal division of the lower/upper Cretaceous transition of the northwestern Black Sea area and Crimea. Abstract of PhD Thesis, Moscow, 18 pp. (in Russian).

Kazmin, V.G, Natapov, L.M. (Eds.), 1998. Paleogeographic Atlas of the Northern Eurasia. Institute of Tectonics of Lithospheric Plates, Moscow, 28 pp.

Kopaevich, L., Kuzmicheva, T., 2002. The Cenomanian–Turonian boundary in southwestern Crimea, Ukraine: Foraminifera and palaeogeographic implications. In: Wagreich, M. (Ed.), Aspects of Cretaceous Stratigraphy and Palaeobiogeography. Osterreichische Akademie der Wissenschaften Schriftenreihe der Erdwissenschaftlichen Kommissionen 15, 129–149.

Kopaevich, L., Vishnevskaya, V., 2016. Cenomanian–Campanian (Late Cretaceous) planktonic assemblages of the Crimea-Caucasus area: Palaeoceanography, palaeoclimate and sea level changes. Palaeogeography, Palaeoclimatology, Palaeoecology 441 (3), 493–515.

Kopaevich, L.F., Walaszczyk, I., 1993. Inoceramid and planktonic foraminifera stratigraphy of the Turonian–Coniacian sediments of Aksudere section. Moscow University Bulletin. Series 4. Geology 1, 70–82 (in Russian).

Kuzmicheva, T.A., 2001. Foraminifer distribution at the Cenomanian–Turonian transition in the Mt. Belaya section, southwestern Crimea. Moscow University Bulletin. Series 4. Geology 4, 27–35 (in Russian).

Lamolda, M.A., Gorostidi, A., Paul, C.R.C., 1994. Quantitative estimates of calcareous nannofossil changes across the Plenus Marls (latest Cenomanian), Dover, England: Implications for the generation of the Cenomanian–Turonian boundary event. Cretaceous Research 15 (2), 143–164.

Lamolda, M.Z., Paul, C.R.C., Peryt, D., Pons, J.M., 2014. The Global Boundary Stratotype and Section Point (GSSP) for the base of the Santonian Stage, "Cantera de Margas", Olazagutia, northern Spain. Episodes 37 (1), 2–13.

Lees, J.A., 2007. New and rarely reported calcareous nannofossil from the Late Cretaceous of coastal Tanzania: outcrop samples and Tanzania Drilling Project Sites 5, 9 and 15. Journal of Nannoplankton Research 29, 39–65.

Lees, J.A., 2008. The calcareous nannofossil record across the Late Cretaceous Turonian/Coniacian boundary, including new data from Germany, Poland, the Czech Republic and England. Cretaceous Research 29, 40–64.

Lees, J.A., Bown, P.R., Mattioli, E., 2005. Problems with proxies? Cautionary tales of calcareous nannofossil paleoenvironmental indicators. Micropaleontology 51 (4), 333–343.

Linnert, C., Mutterlose, J., Erbacher, J., 2010. Calcareous nannofossils of the Cenomanian/Turonian boundary interval from the Boreal Realm (Wunstorf, Northwest Germany). Marine Micropaleontology 74, 38–58.

Lowery, C.M., Corbett, M.J., Leckie, R.M., Watkins, D., Miceli Romero, A., Pramudito, A., 2014. Foraminiferal and nannofossil paleoecology and paleoceanography of the Cenomanian–Turonian Eagle Ford Shale of southern Texas. Palaeogeography, Palaeoclimatology, Palaeoecology 413 (1), 49–65.

Luciani, V., Cobianchi, M., 1999. The Bonarelli Level and other black shales in the Cenomanian–Turonian of the northeastern Dolomites (Italy): calcareous nannofossil and foraminiferal data. Cretaceous Research 20, 135–167.

Maslakova, N.I., 1959. Upper Cretaceous stratigraphic scheme of Crimea. Moscow University Bulletin. Series 4. Geology 1, 109–113 (in Russian).

Maslakova, N.I., 1978. Globotruncanids of the South of European Part of the USSR. Nauka Publishing House, Moscow, 168 pp. (in Russian).

Matveev, A.V., 2013. Upper Cretaceous nannofossil stratigraphy of the Mountain Crimea. Geological Journal 4, 46–51.

Melinte, M.C., Lamolda, M.A., 2007. Calcareous nannofossil biostratigraphy of the Coniacian/Santonian boundary interval in Romania and

comparison with other European regions. Cretaceous Research 28 (1), 119–127.

Melinte-Dobrinescu, M.C., Bojar, A.-V., 2008. Biostratigraphic and isotopic record of the Cenomanian–Turonian deposits in the Ohaba-Ponor section (SW Hatxeg, Romania). Cretaceous Research 29, 1024–1034.

Melinte-Dobrinescu, M.C., Bernardez, E., Kaiho, K., Lamolda, M.A., 2013. Cretaceous Oceanic Anoxic Event 2 in the Arobes section, northern Spain: nannofossil fluctuations and isotope events. In: Bojar, A.-V., Melinte-Dobrinescu, M.C., Smit, J. (Eds.), Isotopic Studies in Cretaceous Research. Geological Society, London, Special Publications 382, 63–84.

Naydin, D.P., 2004. Marl-limestone couplets of the Crimean Cenomanian — indicators of different paleogeographic regimes of precessional semi-cycles. Izvestiâ vyssih učebnyh zavedenij. Geologiâ i razvedka 1, 12–17 (in Russian).

Nikishin, A.M., Wannier, M., Alekseev, A.S., Almendinger, O.A., Fokin, P.A., Gabdullin, R.R., Khudoley, A.K., Kopaevich, L.F., Mityukov, A.V., Petrov, E.I., Rubtsova, E.V., 2015. Mesozoic to recent geological history of southern Crimea and the Eastern Black Sea region. In: Sosson, M., Stephenson, R.A., Adamia, S.A. (Eds.), Tectonic Evolution of the Eastern Black Sea and Caucasus. Geological Society, London, Special Publications 428, 241–264.

O'Connor, L.K., Jenkyns, H.C., Robinson, S.A., Remmelzwaal, S.R.C., Batenburg, S.J., Parkinson, I.J., Gale, A.S., 2020. A re-evaluation of the Plenus cold event, and the links between CO_2, temperature, and seawater chemistry during OAE 2. Paleoceanography and Paleoclimatology 35, e2019PA003631.

Ovechkina, M.N., Kopaevich, L.F., Aleksandrova, G.N., Proshina, P.A., Ryabov, I.A., Baraboshkin, E.Yu., Guzhikov, A.Yu., Mostovski, M. B., 2021. Calcareous nannofossils and other proxies define the Santonian–Campanian boundary in the Central Crimean Mountains (Alan-Kyr section). Cretaceous Research 119, 104706.

Perch-Nielsen, K., 1985. Mesozoic calcareous nannofossils. In: Bolli, H. M., Saunders J.B., Perch-Nielsen, K. (Eds.), Plankton Stratigraphy. Cambridge University Press, Cambridge, pp. 423–554.

Reboulet, S., Giraud, F., Colombié, C., Carpentier, A., 2013. Integrated stratigraphy of the Lower and Middle Cenomanian in a Tethyan section (Blieux, southeast France) and correlations with Boreal basins. Cretaceous Research 40, 170–189.

Robaszynski, F., Gale, A., Juignet, P., Amédro, F., Hardenbol, J., 1998. Sequence stratigraphy in the Upper Cretaceous Series of the Anglo-Paris Basin: Exemplified by the Cenomanian Stage. In: Graciansky, P.-C., Hardenbol, J., Jacquin, T., Vail, P.R. (Eds.), Mesozoic and Cenozoic Sequence Stratigraphy of European Basins. SEPM Special Publication 60, 363–386.

Roth, P.H., Bowdler, J.L., 1979. Evolution of the calcareous nannofossil genus *Micula* in the late Cretaceous. Micropaleontology 25 (3), 272–280.

Shcherbinina, E.A., Gavrilov, Yu.O., 2016. Cenomanian to Santonian nannofossil stratigraphy of SW Crimea. In: Baraboshkin, E.Yu. (Ed.), Cretaceous System of Russia and CIS Countries: Problems of Stratigraphy and Paleogeography. Proceedings of the 8th All-Russian Meeting, 26 September–3 October 2016, Republic of Crimea, Simferopol. Chernomorpress Publishing House, Simferopol, pp. 292–294.

Shumenko, S.I., Stetsenko, V.P., 1978. Zonal division of the upper Cretaceous sediments of Crimea using nannofossil zonation. Reports of Academy of Sciences of USSR 241 (5), 1160–1162.

Sissingh, W., 1977. Biostratigraphy of Cretaceous calcareous nannoplankton. Geologie en Mijnbouw 56 (1), 37–65.

Ustinova, M.A., Gabdullin, R.R., 2019. Calcareous nannoplankton of Cretaceous rocks of the Bakhchisarai region of Southwest Crimea. Moscow University Geology Bulletin 74 (2), 173–184.

Yudin, V.V., 2018. Geological Map and Sections of the Mountainous and Piedmont Crimea, Scale 1:200,000. Cartographic Factory of VSGEI, Saint-Petersburg, 2 pp.

Vishnevskaya, V.S., Kopaevich, L.F., Beniamovskii, V.N., Ovechkina, M. N., 2018. The correlation of the Upper Cretaceous zonal schemes of the eastern European Platform based on foraminifera, radiolaria, and nannoplankton. Moscow University Geology Bulletin 73 (2), 131–140.

Voigt, S., Gale, A.S., Voigt, T., 2006. Sea-level change, carbon cycling and palaeoclimate during the Late Cenomanian of northwest Europe; an integrated palaeoenvironmental analysis. Cretaceous Research 27, 836–858.

Wagreich, M., Bojar, A.V., Sachsenhofer, R.F., Neuhuber, S., Egger, H., 2008. Calcareous nannoplankton, planktonic foraminiferal, and carbonate carbon isotope stratigraphy of the Cenomanian–Turonian boundary section in the Ultrahelvetic Zone (Eastern Alps, Upper Austria). Cretaceous Research 29, 965–975.

Walaszczyk, I., Wood, C.J., Lees, J.A., Peryt, D., Voigt, S., Wiese, F., 2010. The Salzgitter-Salder Quarry (Lower Saxony, Germany) and Słupia Nadbrzeżna river cliff section (central Poland): a proposed candidate composite Global Boundary Stratotype Section and Point for the Coniacian Stage (Upper Cretaceous). Acta Geologica Polonica 60 (4), 445–477.

Wiese, F., Wilmsen, M., 1999. Sequence stratigraphy in the Cenomanian to Campanian of the North Cantabrian Basin (Cantabria, N-Spain). Neues Jahrbuch für Geologie und Paläontologie – Abhandlungen 212, 131–173.

Wiese, F., Košták, M., Wood, C.J., 2009. The Upper Cretaceous belemnite *Preaactinocamax plenus* (Blainville, 1827) from Lower Saxony (Upper Cenomanian, northwest Germany) and its distribution pattern in Europe. Paläontologische Zeitschrift 83, 309–321.

Wilmsen, M., 2007. Integrated stratigraphy of the upper Lower–lower Middle Cenomanian of northern Germany and southern England. Acta Geologica Polonica 57 (3), 263–279.

Wilmsen, M., 2012. Origin and significance of Late Cretaceous bioevents: Examples from the Cenomanian. Acta Palaeontologica Polonica 57 (4), 759–771.

Wilmsen, M., Voigt, T., 2006. The middle–upper Cenomanian of Zilly (Sachsen-Anhalt, northern Germany) with remarks on the Pycnodonte Event. Acta Geologica Polonica 56 (1), 17–31.

Wilmsen, M., Niebuhr, B., Hiss, M., 2005. The Cenomanian of northern Germany: facies analysis of a transgressive biosedimentary system. Facies 51, 242–263.

Wilmsen, M., Schumacher, D., Niebuhr, B., 2021. The early Cenomanian *crippsi* Event at Lüneburg (Germany): palaeontological and stratigraphical significance of a widespread Late Cretaceous bioevent. Palaeobiodiversity and Palaeoenvironments 101, 927–946.

Wind, F.H., 1979. Maestrichtian–Campanian nannofloral provinces of the southern Atlantic and Indian Oceans. In: Talwani, M., Hay, W.W., Ryan, W.B.F. (Eds.), Deep Drilling Results in the Atlantic Ocean: Continental Margins and Paleoenvironment. American Geophysical Union, Washington, pp. 123–137.